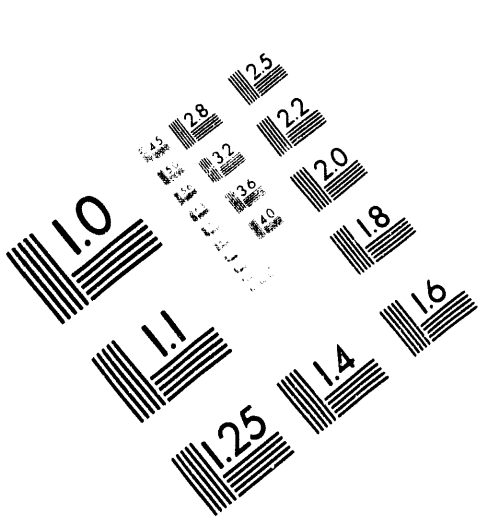

Association for Information and Image Management
1100 Wayne Avenue, Suite 1100
Silver Spring, Maryland 20910
301/587-8202

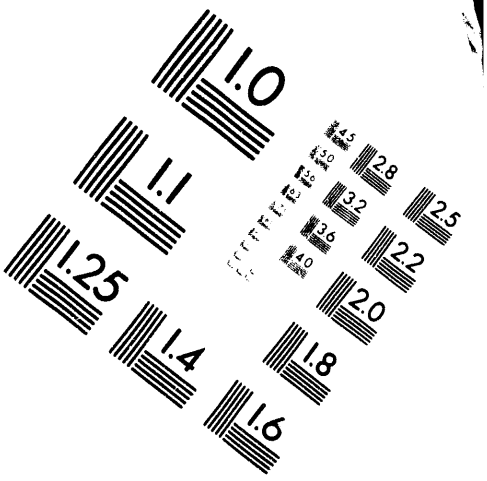

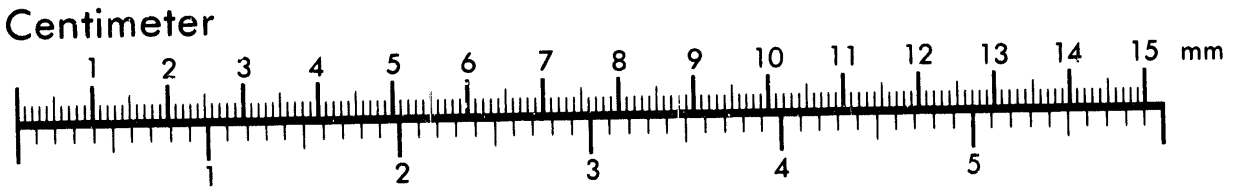

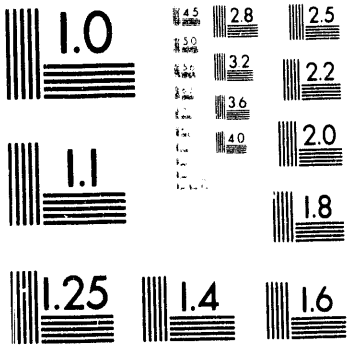

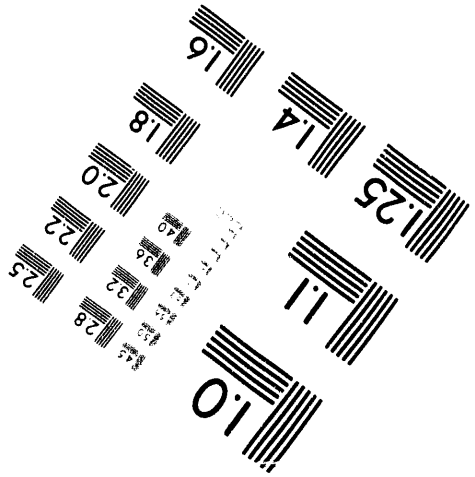

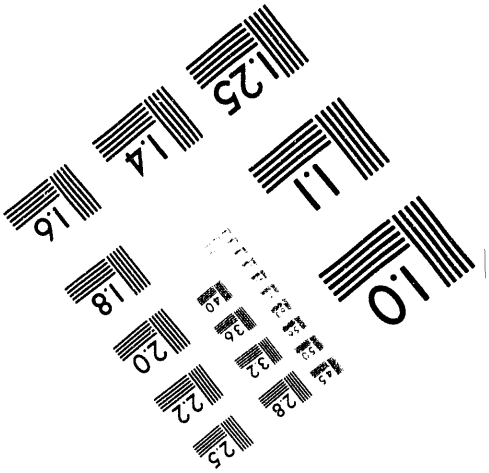

1 of 1

DOE/ID/12934-17

ADSORPTION OF WATER VAPOR ON RESERVOIR ROCKS

QUARTERLY REPORT

FIRST QUARTER 1993

PERIOD JANUARY THRU MARCH 1993

Work Performed Under Contract DE-FG07-90ID12934

For
U. S. Department of Energy
Office of Industrial Technologies
Washington, D.C.

By
Stanford Geothermal Program
Stanford University

DOE/ID/12934-17

ADSORPTION OF WATER VAPOR ON RESERVOIR ROCKS

QUARTERLY REPORT FOR JANUARY-MARCH 1993

July 1993

Work Performed Under Contract No. DE-FG07-SOID12934

Prepared for the
U.S. Department of Energy
Under DOE Idaho Operations Office
Sponsored by the Office of the Assistant Secretary
for Energy Efficiency and Renewable Energy
Office of Industrial Technologies
Washington, D.C.

Prepared by
Stanford Geothermal Program
Stanford University

Quarterly Report for January-March 1993

Stanford Geothermal Program
Stanford University

May 13, 1993

1 ADSORPTION OF WATER VAPOR ON RESERVOIR ROCKS

This experimental project is under the direction of Research Associate, Dr. Shubo Shang, and Professor Henry J. Ramey, Jr. The focus of the work is the experimental investigation of adsorption of water onto geothermal reservoir rocks.

The results of water adsorption/desorption tests performed on Geysers shallow reservoir cores, Berea sandstone and Montiverdi #2 samples were reported previously in the Stanford Geothermal Program Second Annual Technical Report and July–Sept. Quarterly Report (1992). In our continued effort to collect water adsorption/desorption data on a wide range of reservoir samples, we have performed a test on one of the samples from ENEL, Italy. This sample of well cuttings is from Monteverdi #2. The results of this test, reported in Oct.–Dec. Quarterly Report (1992), are in general agreement with those obtained previously on another Monteverdi #2 sample.

As described in the Oct.–Dec. Quarterly Report (1992), problems in the heating system of the sorptometer made the measured adsorption isotherm at high relative pressures inaccurate. We have implemented the heating system by replacing the previous heater with flexible cable heaters. With the flexible cable heaters, we have a better temperature control and have eliminated the condensation problem we had before. We are now able to run adsorption tests at relative pressures beyond 0.9 for temperatures up to $130°C$. The results obtained on a Geysers sample is summarized here.

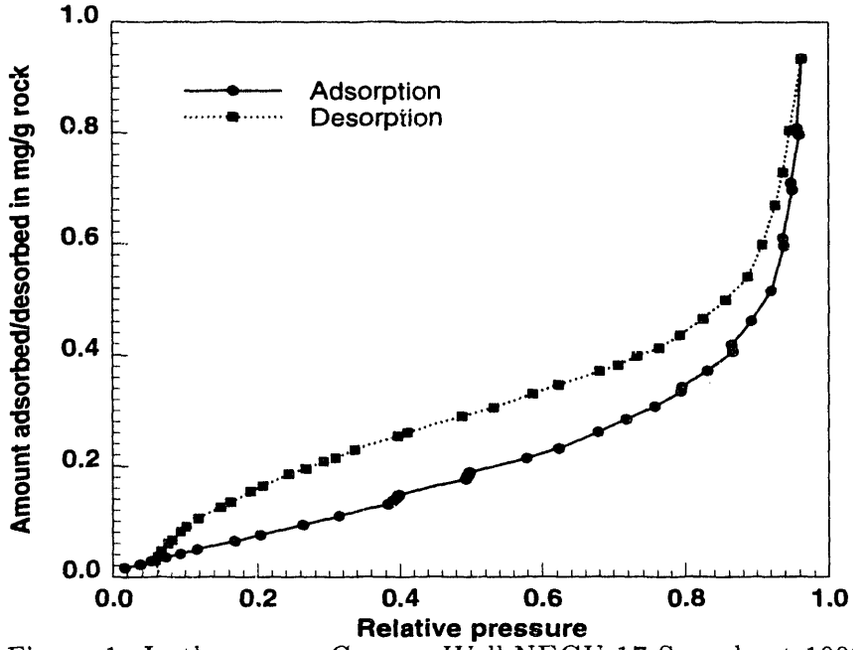

Figure 1: Isotherms on Geysers Well NEGU-17 Sample at $100°C$

Figures 1 and 2 show the adsorption/desorption isotherms obtained at 100° and 120°C on Geysers sample from well NEGU-17. As shown in the figures, the amount of water adsorbed at low relative pressure is low. As relative pressure increases, the amount of water adsorbed increases rapidly. The changes in the curvature of the adsorption isotherms indicate changes of process mechanism from adsorption dominant to the presence of both adsorption and capillary condensation. Hysteresis exists in water vapor adsorption/desorption on Geysers well NEGU-17 sample, similar to those reported previously. The origin of the hysteresis is not yet clear to us.

Figure 3 compares the adsorption isotherms obtained on this sample at temperatures of 80, 100, 120 and 130°C. As shown in the figure, the temperature has a clear influence on the amount of water adsorbed for relative pressures below 0.3. For intermediate relative pressures, the amount adsorbed increases with temperature. For relative pressures beyond 0.9, the effect of temperature on the isotherm is less clear. Further tests are required to determine the temperature effects at high relative pressures.

Currently, we are running repeated tests on the Geysers sample in order to understand the temperature effect at high relative pressures. It is possible

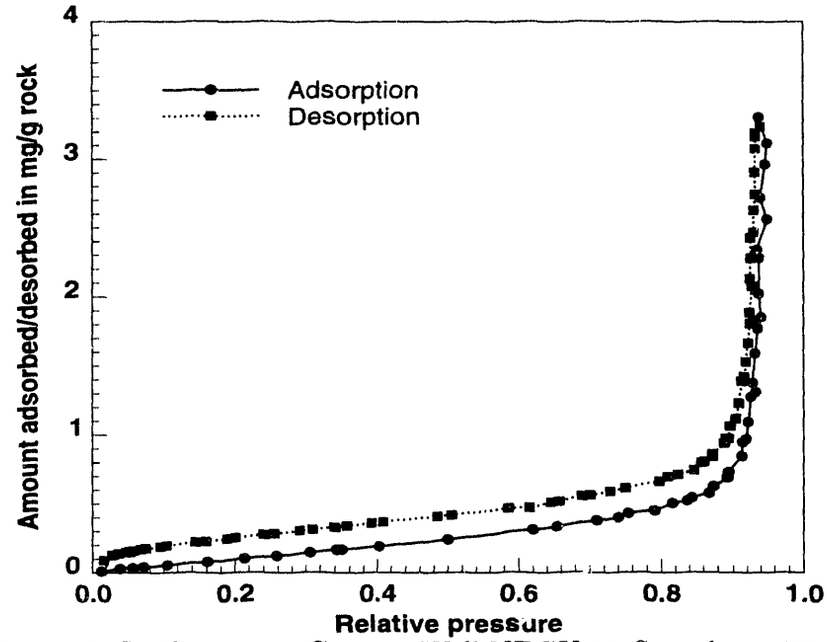

Figure 2: Isotherms on Geysers Well NEGU-17 Sample at $120°C$

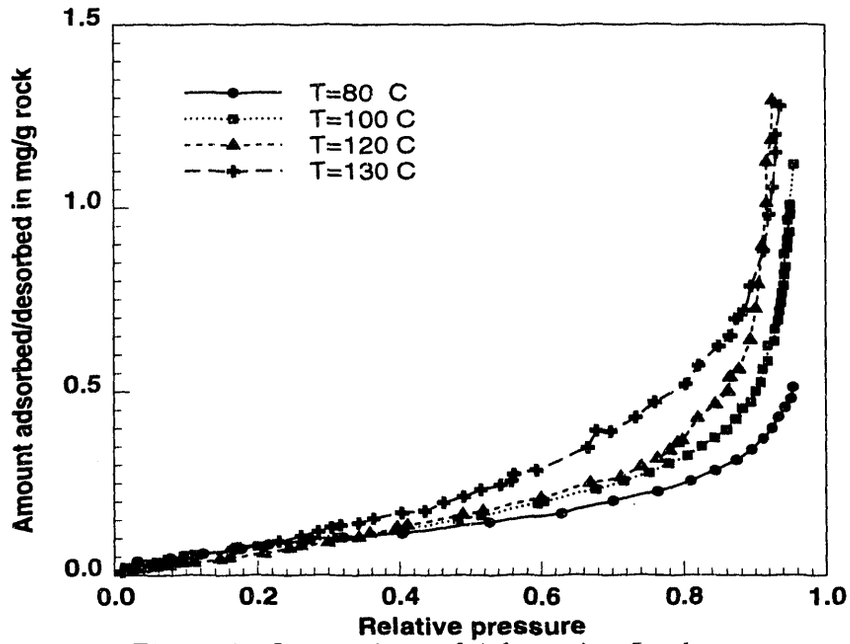

Figure 3: Comparison of Adsorption Isotherms

that the present version of the software is still not able to handle the experiment accurately at high relative pressures. If this is the case, we will have to work together with engineers from Porous Materials, Inc. We also plan to obtain isotherms on the samples previously used with emphasis on relative pressures higher than 0.8.

2 THEORETICAL INVESTIGATION OF ADSORPTION

This study is under the direction of Professors Antonio Correa and Henry J. Ramey, Jr.

2.1 Introduction

Recent research has supported the idea that, although a vapor gradient could exist at reservoir conditions in a vapor-dominated geothermal reservoir, a large amount of water could be stored in the reservoir as a dense phase, physically and chemically absorbed in the rock surface, and also condensed into small pores due to capillary effects.

Although the mechanism of adsorption in very irregular and heterogeneous surfaces such as the pore interiors is not fully understood, laboratory experiments can provide useful information on the amount of water absorbed as function of pressure and temperature. At pressures near the vapor pressure of water at reservoir temperature, the effect of capillary condensation is dominant. However, from a practical point of view, adsorption and capillary condensation can be considered indistinct phenomena because their effects act in the same direction, that is, both increase the amount of water present as a dense phase as pressure increases.

Desorption isotherms obtained from a given reservoir rock may be combined with computer modeling to forecast production of geothermal reservoirs. On the other hand, pressure and cumulative production data of mature geothermal fields could also be used to yield information on the amount of liquid water existing in such reservoirs.

In this work, we explore the feasibility of using field data to quantify the amount water adsorbed or capillary condensed in geothermal reservoirs.

2.2 Material Balance Equation

We consider isothermal flow in the reservoir, allowing for water vaporization to take place at a constant temperature. This may be the case in fractured reservoirs with low matrix porosity, where most of the heat is stored in the water bearing rock.

A material balance of the reservoir water yields:

$$\frac{\partial m}{\partial t} + \dot{m} = 0 \,, \tag{1}$$

in which m is the mass of water in the reservoir at time t and $\dot{m}$ is the net rate of mass withdrawal.

The mass of resident water existing in a unit bulk volume of reservoir is given by:

$$m = \phi_m \left[\rho_w S_{wm} + \rho_v (1 - S_{wm})\right] + \phi_f \rho_v \,, \tag{2}$$

in which the S denotes saturation, ρ denotes density and ϕ is the porosity. The subscripts w and v refer to water in liquid and vapor states, and the subscripts f and m refer to fracture and matrix, respectively. Eq. 2 is valid for pressures less than the vapor pressure as it considers the fractures to be fully vapor saturated.

Since we are considering the dense water phase as adsorbed or condensed into the rock matrix, we assume no flow of liquid water in the reservoir. Steam produced by vaporization of liquid water in the matrix moves towards the flowing stream of superheated steam in the fracture network.

Both experimental and theoretical works support the conclusion that the amount of absorbed water is a function of pressure and temperature. Also, capillary condensation is known to be dependent on pressure and temperature. Bearing this fact in mind we can combine Eqs. 1 and 2 and consider both densities and saturation to be functions of the reservoir pressure, to obtain:

$$\dot{m} = -V_b \left[\phi_m \frac{\partial(\rho_w - \rho_v) S_{wm}}{\partial p} + (\phi_m + \phi_f) \frac{\partial \rho_v}{\partial p}\right]_T \frac{dp}{dt} \,, \tag{3}$$

in which V_b is the reservoir bulk volume and the porosities are considered to be invariant with pressure.

We assume that initially the reservoir is at a pressure less than the vapor pressure, such that $S_{wm}(p_i) = S_{wmi}$. Equation 3 can be integrated from the beginning of the exploitation to yield the cumulative mass produced at an arbitrary pressure:

$$\begin{aligned} m_p = {} & V_p \{(1-\omega) S_{wmi} \rho_{wi} + [1-(1-\omega) S_{wmi}] \rho_{vi}\} \\ & - V_p \{(1-\omega) S_{wm} \rho_w + [1-(1-\omega) S_{wm}] \rho_v\} \end{aligned} \tag{4}$$

where V_p is the reservoir pore volume, $\omega = \phi_f/(\phi_m + \phi_f)$ is the fracture porosity fraction, and the subscript i denotes initial conditions. Note in Eq. 4 that $m_i = V_p \{(1-\omega) S_{wmi} \rho_{wi} + [1-(1-\omega) S_{wmi}] \rho_{vi}\}$ representing the initial mass of water in place.

The fractional cumulative mass production m_p/m_i can be computed from Eq. 4, yielding:

$$\frac{m_p}{m_i} = 1 - \frac{(1-\omega) S_{wm} \rho_w + [1-(1-\omega) S_{wm}] \rho_v}{(1-\omega) S_{wmi} \rho_{wi} + [1-(1-\omega) S_{wmi}] \rho_{vi}} . \tag{5}$$

Recall that the derivation presented in this section applies to isothermal exploitation of geothermal reservoirs. Under water injection, additional heat may be extracted by cooling of reservoir rock, so proper modeling requires an energy balance to be performed.

We seek a relation between matrix water content and pressure, which may be useful to determine the mass of water in the reservoir from the analysis of data obtained during a depletion process. Both adsorption and capillary condensation mechanisms will be investigated.

2.3 Capillary Condensation

Consider a porous matrix in which a thin layer of water has been adsorbed onto the pore walls. Although the amount of water adsorbed changes with pressure, for the time being we will consider the thickness of the adsorbed layer to be negligible compared to the pore dimensions.

The adsorbed layer prevents direct contact of the vapor with the rock, leading to a curved vapor-liquid interface inside the pores. This causes a pressure difference across the interface, resulting in the lowering of the vapor

pressure of the water and in the premature condensation of the water in the pore. Such capillary condensation effects are usually quantifyed by the Kelvin equation:

$$\ln \frac{p}{p_s} = -\frac{2\sigma v_l}{RT}\frac{1}{r_m} , \tag{6}$$

in which r_m is the mean radius of curvature of the interface, p_s is the flat-interface vapor pressure at the absolute temperature T, σ is the liquid-vapor interfacial tension, v_l is the molar volume of the liquid and R is the universal gas constant. Note that for a flat interface, such that $r_m \rightarrow \infty$, there are no vapor pressure lowering effects, that is, $p \rightarrow p_s$.

When the pressure acting in the vapor phase is less than the vapor pressure computed by the Kelvin equation, vapor and adsorbed water are assumed to coexist in thermodynamic equilibrium inside of a pore. On the other hand, if pressure in the vapor phase is greater than the computed vapor pressure, the pore will be completely filled with condensed water.

We now consider a porous medium characterized by a given distribution of pore sizes, represented by:

$$\frac{1}{V_{pm}}\frac{dV(r)}{dr} = \lambda(r) , \tag{7}$$

in which V_{pm} is the total pore volume of the matrix, $dV(r)$ is the volume of pores having radii between r and $r + dr$, and $\lambda(r)$ is the probability density of the pore size distribution. A probability density must satisfy the condition $\int_0^\infty \lambda(r)\, dr = 1$.

Throughout this work we consider that the porous medium is represented by a lognormal distribution of pore sizes. We will keep the derivations as general as possible so that extension of the present work to include other types of pore size distributions follows the procedures to be described.

The probability density of the lognormal distribution is given by:

$$\lambda(r) = \frac{1}{\sqrt{2\pi}\,\sigma_y\, r} \exp\left[-\frac{1}{2\,\sigma_y^2}\left(\ln\frac{r}{\mu_y}\right)^2\right] , \tag{8}$$

in which the distribution parameters are the median μ_y and the shape parameter σ_y, the latter being the standard deviation of the logarithm of the lognormal distribution.

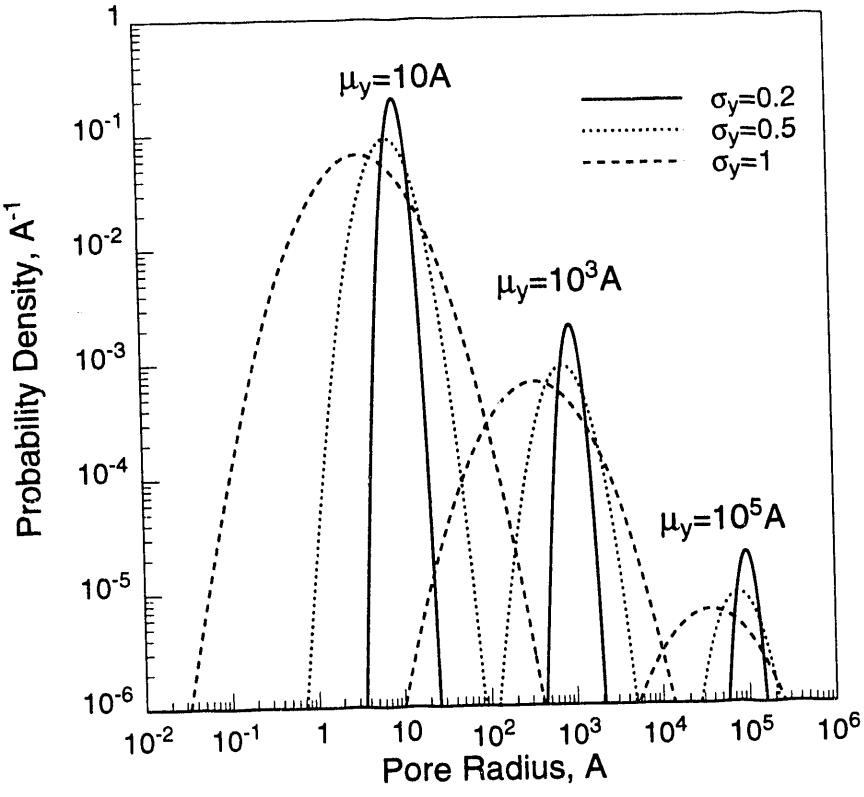

Figure 4: Lognormal Probability Density

Figure 4 displays the probability density of lognormal pore size distribution as a function of the pore radius for a few combinations of the model parameters. Note that μ_y translates the distribution while σ_y is a measure of pore size dispersion.

Equation 7 can be integrated to yield the fraction of the pore volume having radii less than an arbitrary radius, that is:

$$\frac{V(r)}{V_{pm}} = \int_0^r \lambda(r)\, dr \ . \tag{9}$$

which, for the lognormal distribution defined by Eq. 8, results in:

$$\frac{V(r)}{V_{pm}} = \frac{1}{2} + \frac{1}{2}\,\mathrm{erf}\left[\frac{1}{\sqrt{2}\,\sigma_y}\ln\left(\frac{r}{\mu_y}\right)\right] \ . \tag{10}$$

Figure 5 presents the normalized cumulative pore volume as a function of the pore size for the same model parameters used to generate Fig.4.

A relation between liquid saturation and pressure may be obtained by recalling that, for a given vapor phase pressure, all pores with radii less than

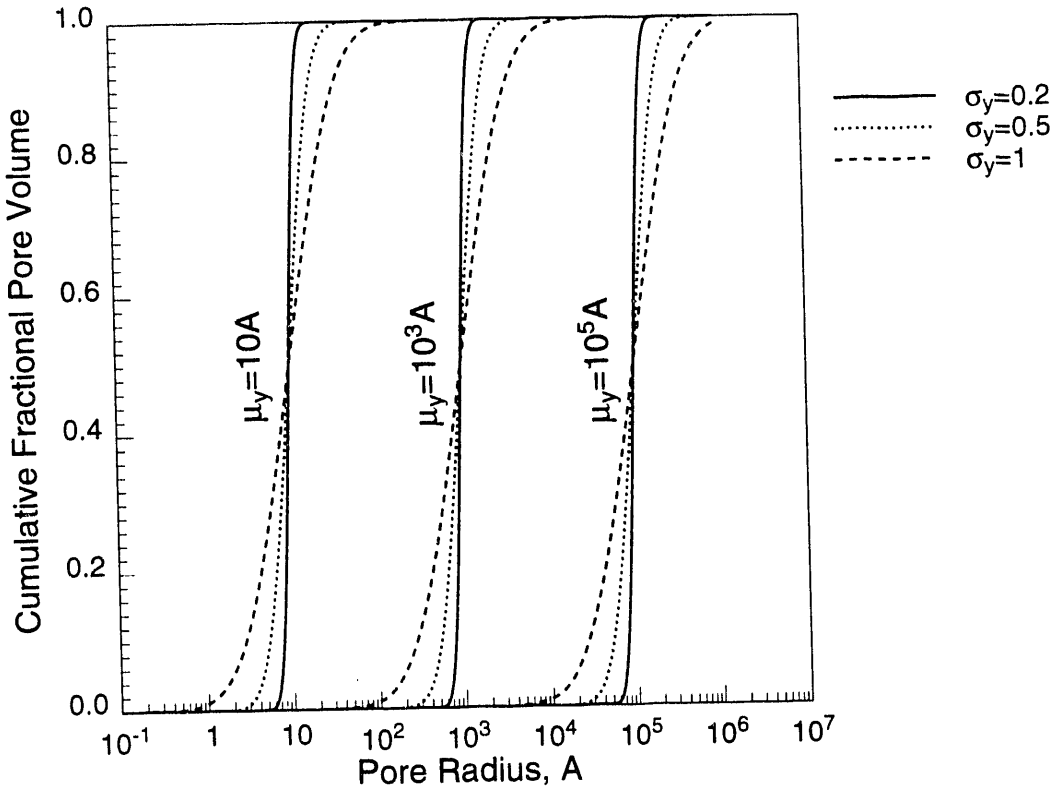

Figure 5: Lognormal Cumulative Frequency

the pore radius computed from the Kelvin equation are filled with condensed water. This implies that, in this case, $S_{wm} = V(r)/V_{pm}$, allowing Eqs. 6 and 10 to be combined to yield the following expression for the water saturation:

$$S_{wm} = \frac{1}{2} + \frac{1}{2}\,\mathrm{erf}\left[\frac{1}{\sqrt{2}\,\sigma_y}\ln\left(-\frac{2\,\sigma\,v_l}{\mu_y\,R\,T\,\ln p/p_s}\right)\right]. \qquad (11)$$

From Eq. 11 we infer that, for a reservoir at isothermal conditions, the liquid saturation in the matrix depends only on the relative pressure p/p_s.

Note in Eq. 11 that the argument of the logarithm function is a dimensionless quantity. Thus, only two parameters affect the capillary condensation isotherm, which are σ_y and a dimensionless capillary radius defined as follows:

$$r_D = \frac{2\,\sigma\,v_l}{\mu_y\,R\,T}. \qquad (12)$$

Using this definition, Eq. 11 reduces to:

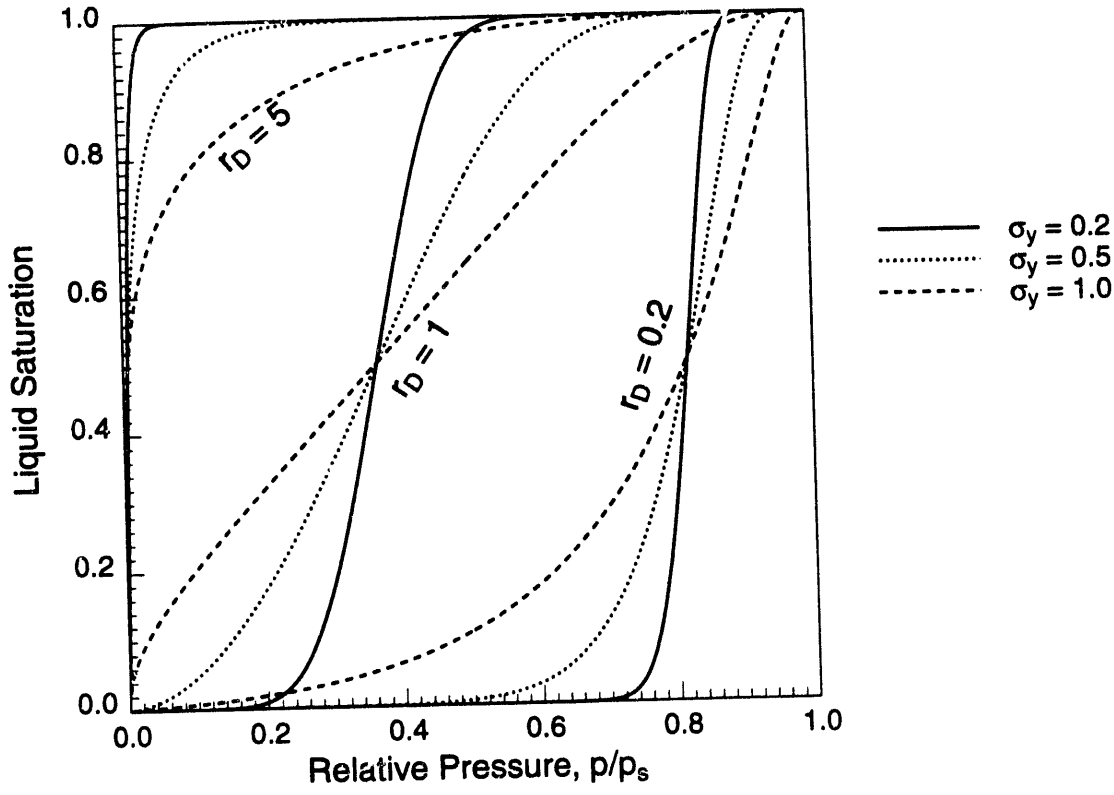

Figure 6: Capillary Condensation Isotherm

$$S_{wm} = \frac{1}{2} + \frac{1}{2}\,\mathrm{erf}\left[\frac{1}{\sqrt{2}\,\sigma_y}\ln\left(-\frac{r_D}{\ln p/p_s}\right)\right] . \qquad (13)$$

Figure 6 displays the water saturation as function of the relative pressure for r_D values of 0.2, 1 and 5, and σ_y values of 0.2, 0.5 and 1.

The effect of temperature on the capillary condensation isotherm is presented in Fig. 7. According to the Kelvin equation, for a fixed relative pressure, the upper limit of capillary radius at which condensation may take place is proportional to $\sigma v_l/T$. Both the molar volume of water and the water-steam interfacial tension decrease with an increase in temperature. Hence, as temperature goes up, the Kelvin equation predicts that condensation takes place at smaller radii, reducing the amount of water condensed at constant relative pressure.

Laboratory experiments have shown that the effect of temperature on capillary condensation is opposite to that predicted by the Kelvin equation. This is somewhat surprising, and because the structure of the pore system remains unchanged, the explanation for such observed phenomena must lay

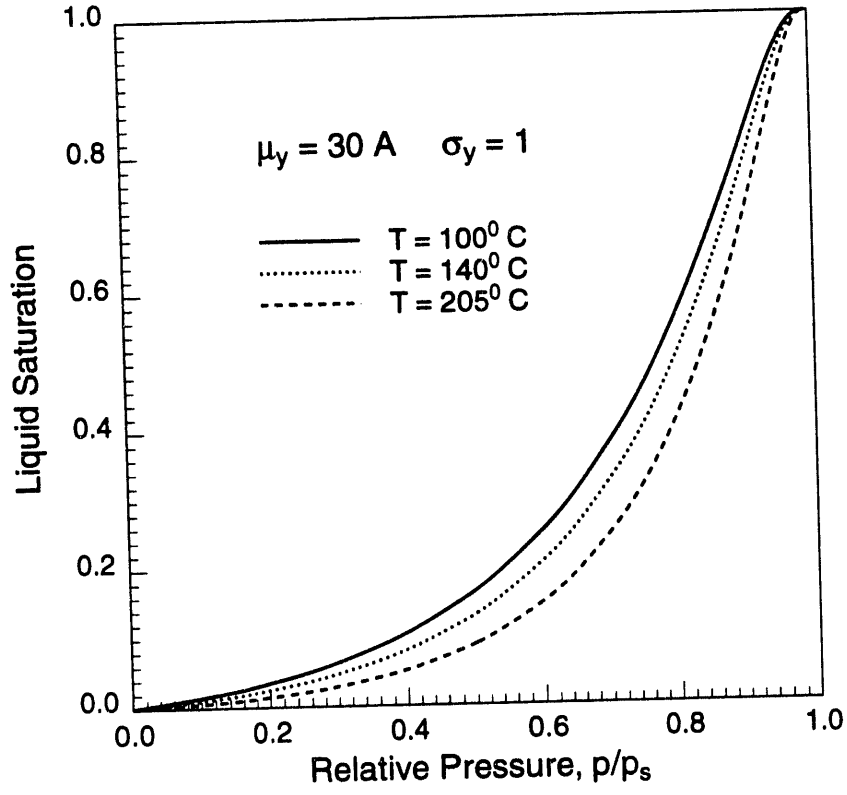

Figure 7: Effect of Temperature on Capillary Condensation

in the change of the vapor properties with temperature.

2.4 The Concept of Critical Capillary Radius

The volume occupied by a liquid molecule is very small, as it may easily fit into the micropores of a solid. The equivalent radius of a liquid molecule, r_w, can be computed by:

$$r_w = \left[\frac{3\,v_l}{4\pi\,N_A}\right]^{1/3}, \tag{14}$$

where N_A is the Avogadro number. For water at ambient conditions, r_w is of the order of 2 Å. This indicates that the thickness of a monolayered adsorbed water film must be close to 4 Å.

Gas molecules require more space to move. The average radius of the space spanned by a gas molecule can be computed from the gas law, giving:

$$r_g = \left(\frac{3\,Z\,RT}{4\pi\,N_A\,p_s}\right)^{1/3}\left(\frac{p}{p_s}\right)^{-1/3}, \tag{15}$$

where Z is the gas deviation factor. For water at 100^0 C the computed value of r_s is 23 Å, which is one order of magnitude larger than r_w.

In pores with radii less than r_g a vapor molecule does not have the same space to move as it has in a continuous vapor phase at same pressure and temperature. Hence, if a gas molecule is present in such pores, the effective pressure acting on it is larger than pressure in the gas phase, leading to a non-equilibrium condition. In view of this fact, we must admit that vapor and liquid can only coexist in equilibrium in pores with dimensions larger than r_g. This concept puts a lower limit where capillary condensation can take place, that is, in pores with dimensions less than r_g capillary condensation may not occur.

Note from Eq. 15 that r_g decreases as the relative pressure increases. On the other hand, from Eq. 6 we observe that r_m increases as the relative pressure is augmented. Thus, there is a pressure at which r_g and r_m become identical, establishing the point where capillary condensation commences. This pressure may be computed by equating the definitions of r_m and r_g, Eqs. 6 and 15, respectively, yielding the following non-linear relation:

$$\frac{(p/p_s)_c^{1/3}}{\ln (p/p_s)_c} = - N_c \, (Z/Z_s)_c^{1/3} \, , \tag{16}$$

where the subscript c denotes the relative pressure at which capillary condensation begins to take place, and N_c is a dimensionless number given by:

$$N_c = \frac{RT}{2\,\sigma\, v_l} \left(\frac{3\, Z_s\, RT}{4\pi\, N_A\, p_s} \right)^{1/3} \, . \tag{17}$$

When adsorption effects are not considered, the onset of capillary condensation is defined by the condensation number N_c, and it is independent of the porous material. For a given substance, the onset depends on temperature only.

The critical capillary radius, that is, the radius at which capillary condensation begins, can be computed by substituting $(p/p_s)_c$ either in Eqs. 6 or 15, yielding:

$$r_c = - \frac{RT}{2\,\sigma\, v_l \, \ln (p/p_s)_c} = \left(\frac{3\, Z_s\, RT}{4\pi\, N_A\, p_s} \right)^{1/3} (p/p_s)_c^{-1/3} \, . \tag{18}$$

A capillary condensation isotherm, including the concept of critical capillary radius, can be computed by properly modifying Eq. 13 to account for the fact that after condensation begins, the pores with radii less than r_g must contain only an infinitesimal amount of adsorbed water. This leads to the following expression for the water saturation:

$$S_{wm} = \frac{1}{2}\,\mathrm{erf}\left[\frac{1}{\sqrt{2}\,\sigma_y}\ln\left(-\frac{r_D}{\ln p/p_s}\right)\right] - \frac{1}{2}\,\mathrm{erf}\left[\frac{1}{\sqrt{2}\,\sigma_y}\ln\frac{r_g}{\mu_y}\right]. \qquad (19)$$

Equation 19 is valid for $(p/p_s) > (p/p_s)_c$ or $r > r_c$ only. Note, that, since adsorption effects have been neglected, then for $(p/p_s) < (p/p_s)_c$ we have $S_{wm} = 0$.

Figure 8 displays the capillary condensation isotherms computed by means of Eq. 19, with the same parameters used to produce the isotherms of Fig.7. The introduction of the concept of critical capillary radius leads to a remarkable change in the shape of the isotherms, as well as to an inversion of the effect of temperature on capillary condensation as predicted by the Kelvin equation, becoming in agreement with experimental observations.

An interesting feature of this model is that, when capillary condensation commences in a pore with radius r_c, as pressure increases the region of capillary condensation spreads to both larger and smaller pores in the neighborhood of r_c. The capillary condensation region broadens as $p \rightarrow p_s$.

2.5 Adsorption Models

Adsorption can be described as the formation of a dense-phase film of a given substance when the vapor of such substance is brought in contact with a solid surface. The film adheres to the surface preventing the direct contact between the gas and the solid. Physical adsorption is believed to dominate over chemical adsorption in steam and natural gas reservoirs, yielding film thickness of the order of a few molecular layers of the substance being adsorbed (adsorbate). The amount adsorbed, and thus the thickness of the adsorbed film, increases with the increase in the gas phase pressure.

Adsorption is often expressed in terms of mass of adsorbate by mass of solid, as a function of pressure, at constant temperature. The relation between such adsorption isotherms and the liquid saturation is given by:

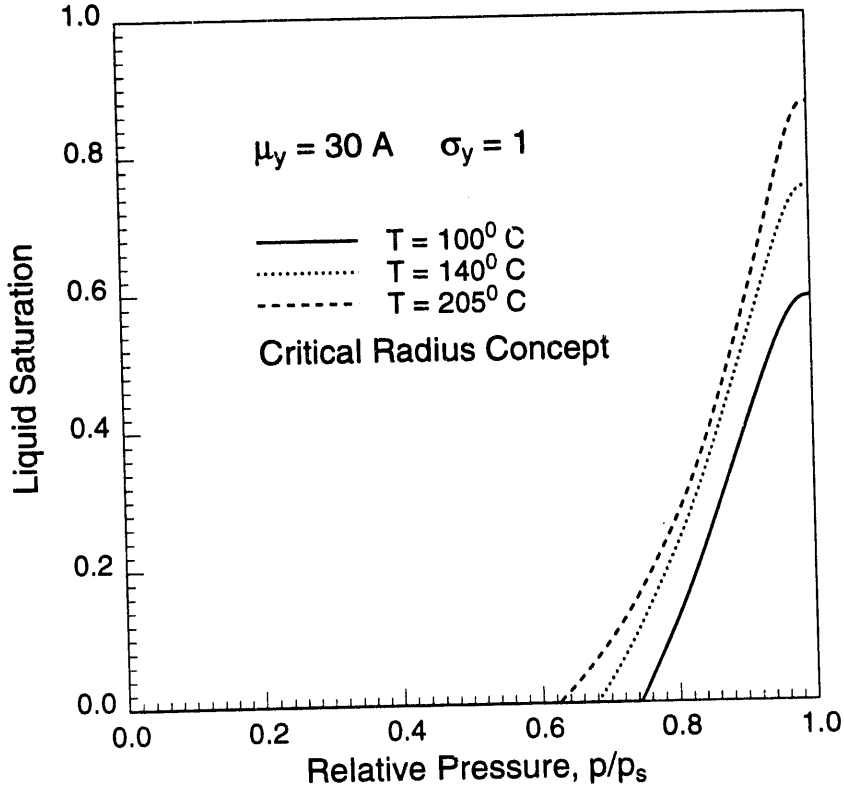

Figure 8: Effect of Temperature on Capillary Condensation - Critical Radius Concept

$$S_{wm} = \frac{1 - \phi_m}{\phi_m} \frac{\rho_r}{\rho_w} X_T(p) \tag{20}$$

in which $X_T(p)$ is the amount adsorbed at pressure p and at constant temperature T, and ρ_r and ρ_w are the solid and liquid densities, respectively.

Among several adsorption models described in the literature, the earliest is due to Langmuir, who quantified the adsorption phenomena as:

$$X_T(p) = \frac{p/p_s}{a + bp/p_s}, \tag{21}$$

where a and b are model parameters and p_s is the vapor pressure at temperature T.

Eq. 21 can be expressed in a more convenient form, as:

$$X_T(p/p_s) = d\frac{cp/p_s}{1 + (c-1)p/p_s}, \tag{22}$$

in which the new model parameters, c and d, are related to those of Eq. 21 by $c = 1 + b/a$ and $d = (a + b)^{-1}$. The parameter c defines the shape of the isotherm and d is the amplification factor.

Figure 9 displays the several forms that the Langmuir isotherm can assume by varying the shape parameter c. Langmuir derived his model by assuming a monolayer coverage of a non-porous surface. A consequence of the original derivation is that the rate of increase in the amount adsorbed should decrease as pressures increases. Therefore, only the isotherms with shapes described by $c > 1$ resembles physical agreement with Langmuir's derivation. However, the Langmuir model has been used to describe adsorption in porous materials, and shapes correspondent to $c < 1$ have been reported in the literature.

For porous materials having pore sizes of the order of several molecular layers of the adsorbate, we expect the Langmuir model to apply at low relative pressures. At high relative pressures, departure of the isotherms from the shapes defined by $c > 1$ have been experimentally verified. However, such deviations from the theoretical model are related to capillary condensation effects and to multilayered film formation.

Brunauer, Emmet and Teller (BET) considered multilayer coverage of the solid surface represented by the following model:

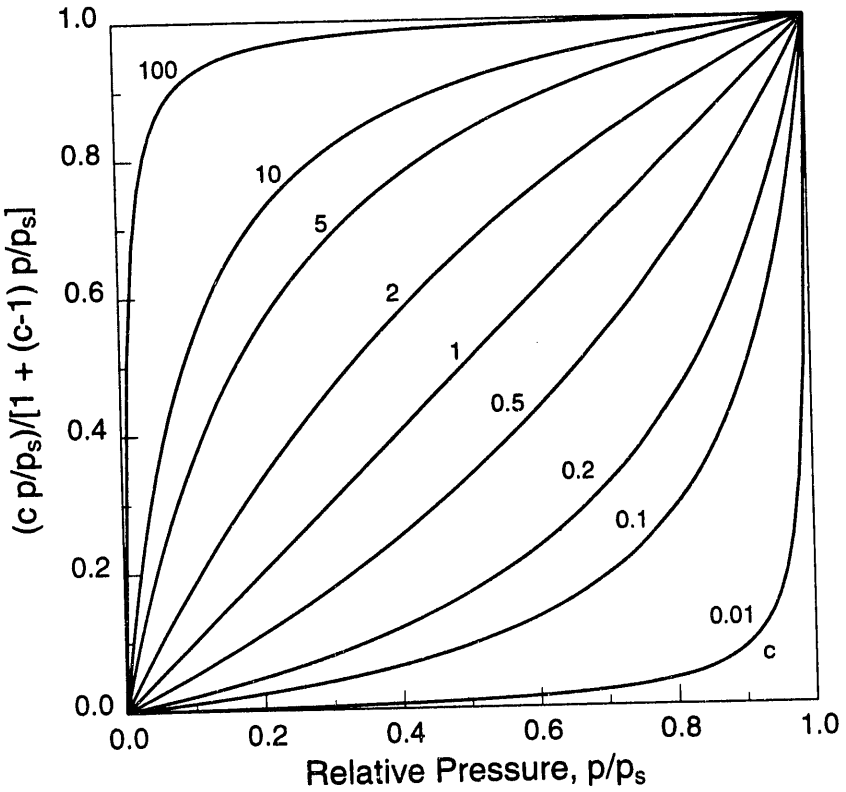

Figure 9: Normalized Langmuir Isotherm

$$X_T(p/p_s) = \frac{d\, c\, p/p_s}{(1 - p/p_s)\,[1 + (c-1)\,p/p_s]}\,. \tag{23}$$

Note in Eq. 23 that for small values of the relative pressure, such that $1 - p/p_s \approx 1$, the BET and the Langmuir models become equivalent. Note also in Eq. 23 that as the relative pressure approaches unity, the amount adsorbed is unlimited. This is because the model described in Eq. 23 is based on an infinite number of layers of the adsorbate, which is not a realistic approach for adsorption in porous materials.

However, both the Langmuir and the BET models can be adapted to represent adsorption in porous materials, which will be discussed next.

2.6 Adsorption in Porous Materials

We consider the case of a spherical pore of radius r, in which a film with an average thickness t_x is adhered to its wall. Derivations for other pore geometries, such as cylindrical or slitted, follow the same development to be presented.

Adsorption causes the film to thicken as the relative pressure increases. The Langmuir model predicts the change in the film thickness by:

$$t_x \;=\; t_m \frac{c\,x}{1+(c-1)\,x}\;, \tag{24}$$

while for the BET model we have:

$$t_x \;=\; t_m \frac{c\,x}{(1-x)\,[1+(c-1)\,x]}\;, \tag{25}$$

where t_m is the thickness of a molecular layer of the adsorbate at pressure p and temperature T, and $x = p/p_s$ is the relative pressure.

By means of a simple geometric construction we can find the adsorbed volume V_x in a pore to be:

$$V_x(r) \;=\; V(r)\left[1 - \left(1 - \frac{t_x}{r}\right)^3\right]\;, \quad r > t_x\;, \tag{26}$$

where $V(r) = \frac{4}{3}\pi r^3$ is the pore volume.

At a fixed relative pressure, the change in the adsorbed volume due to a variation in the pore radius can be obtained by differentiating Eq. 25 and noting that for spherical pores $dV(r) \;=\; 4\pi\, r^2\, dr$:

$$dV_x(r) \;=\; \frac{t_x}{r}\left(2 - \frac{t_x}{r}\right) dV(r)\;, \quad r > t_x\;. \tag{27}$$

We now define the local water saturation $s_x(r)$ as the ratio between the volume of water and the void volume at a given pore size, that is:

$$s_x(r) \;=\; \frac{dV_x(r)}{dV(r)}\;. \tag{28}$$

The overall water saturation in the porous material is defined as the ratio between the total volume of water contained in the pores and the porous volume, or $S_{wm} = \left(\int_0^\infty dV_x(r)\right) / \left(\int_0^\infty dV(r)\right)$. Applying this definition, from Eqs. 7 and 28 we can find the following relation between the local and the overall water saturations:

$$S_{wm} \;=\; \int_0^\infty s_x(r)\,\lambda(r)\,dr\;. \tag{29}$$

For $r < t_x$ all pores are filled with adsorbed water, leading to $s_x(r) = 1$. On the other hand, for $r > t_x$ the local water saturation can be obtained from Eqs. 27 and 28, yielding $s_x(r) = \frac{t_x}{r}\left(2 - \frac{t_x}{r}\right)$. Introducing both values of the local water saturation into Eq. 29 we obtain an expression for the water saturation due to adsorption:

$$S_{wm} = \int_0^{t_x} \lambda(r)\, dr + \int_{t_x}^{\infty} \frac{t_x}{r}\left(2 - \frac{t_x}{r}\right) \lambda(r)\, dr \,. \tag{30}$$

Equation 30 is general and may be used with any distribution of pore sizes. Note that Eq. 30 can also be written as:

$$S_{wm} = 1 + \int_0^{t_x} \left(1 - \frac{t_x}{r}\right)^2 \lambda(r)\, dr - \int_0^{\infty} \left(1 - \frac{t_x}{r}\right)^2 \lambda(r)\, dr \,, \tag{31}$$

in which the property $\int_0^{\infty} \lambda(r)\, dr = 1$ has been used. Denoting $\mathcal{F}_{x,y}$ a function of the pore radius depending on both the pore size distribution and the adsorption model, defined as:

$$\mathcal{F}_{x,y}(r) = \int_0^{r} \left(1 - \frac{t_x}{r'}\right)^2 \lambda(r')\, dr' \,, \tag{32}$$

where r is an arbitrary value and r' is a dummy integration variable, then Eq. 30 can be written in the following form:

$$S_{wm} = 1 + \mathcal{F}_{x,y}(t_x) - \mathcal{F}_{x,y}(\infty) \,. \tag{33}$$

Specifically for a lognormal distribution of pore sizes, substitution of Eq. 8 into Eq. 32 yields the following expression for the function $\mathcal{F}_{x,y}$:

$$\mathcal{F}_{x,y}(r) = \frac{1}{2}\left[1 + \operatorname{erf}\left(\frac{\ln \frac{r}{\mu_y}}{\sqrt{2}\,\sigma_y}\right)\right] - \frac{t_x}{\mu_y} e^{\sigma_y^2/2}\left[1 + \operatorname{erf}\left(\frac{\ln \frac{r}{\mu_y} + \sigma_y^2}{\sqrt{2}\,\sigma_y}\right)\right] + \frac{1}{2}\left(\frac{t_x}{\mu_y}\right)^2 e^{2\sigma_y^2}\left[1 + \operatorname{erf}\left(\frac{\ln \frac{r}{\mu_y} + 2\,\sigma_y^2}{\sqrt{2}\,\sigma_y}\right)\right] \,. \tag{34}$$

Eqs. 33 and 34 can be used to compute the water saturation in porous material showing a lognormal pore size distribution, provided an adsorption model is selected.

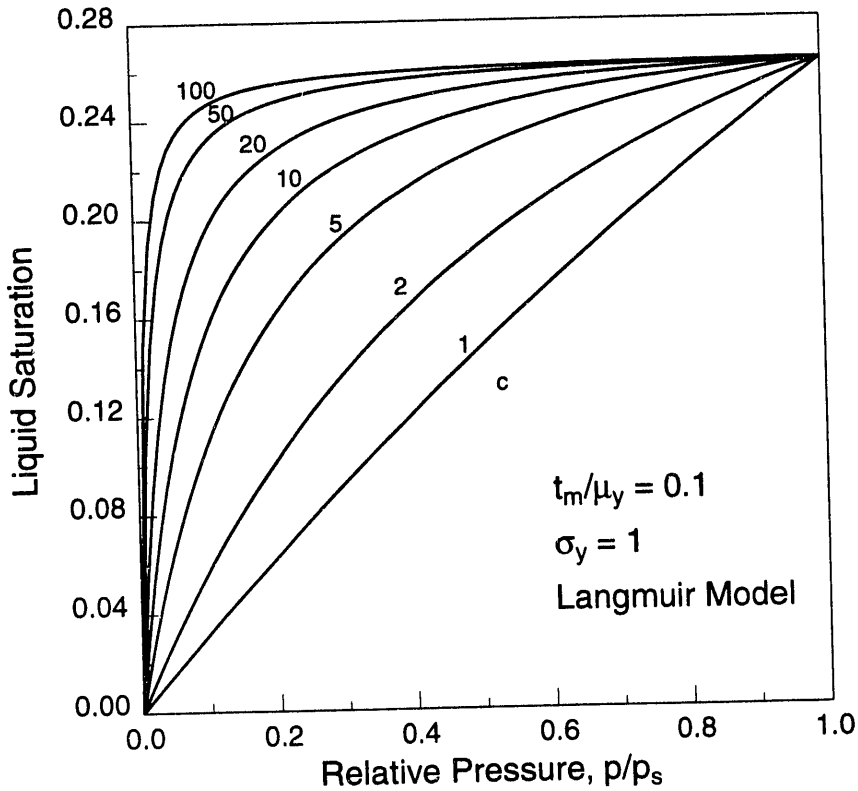

Figure 10: Adsorption in Porous Material - Langmuir Model

Figure 10 displays the computed Langmuir isotherms with $t_m/\mu_y = 0.1$ and $\sigma_y = 1$, for several values of the shape parameter c. Note that the shapes of the isotherms are similar to those of Fig.9, which have been computed assuming adsorption in a non-porous material. An important point appearing in Figure 10 is that the maximum water saturation obtained with the Langmuir model is less than unity, due to the intrinsic assumption of monolayer adsorption. Such maximum saturation value can be computed by making $t_x = t_m$ in Eqs. 33 and 34.

The resulting adsorption isotherms for the BET model are displayed in Figure 11, computed with $t_m/\mu_y = 0.1$ and $\sigma_y = 1$. They have the generic shape observed in the BET isotherms for non-porous solids, but with an important difference - the isotherms for porous materials converge to $S_w = 1$ as p/p_s approaches unity.

At this point, a model combining adsorption and capillary condensation can be devised.

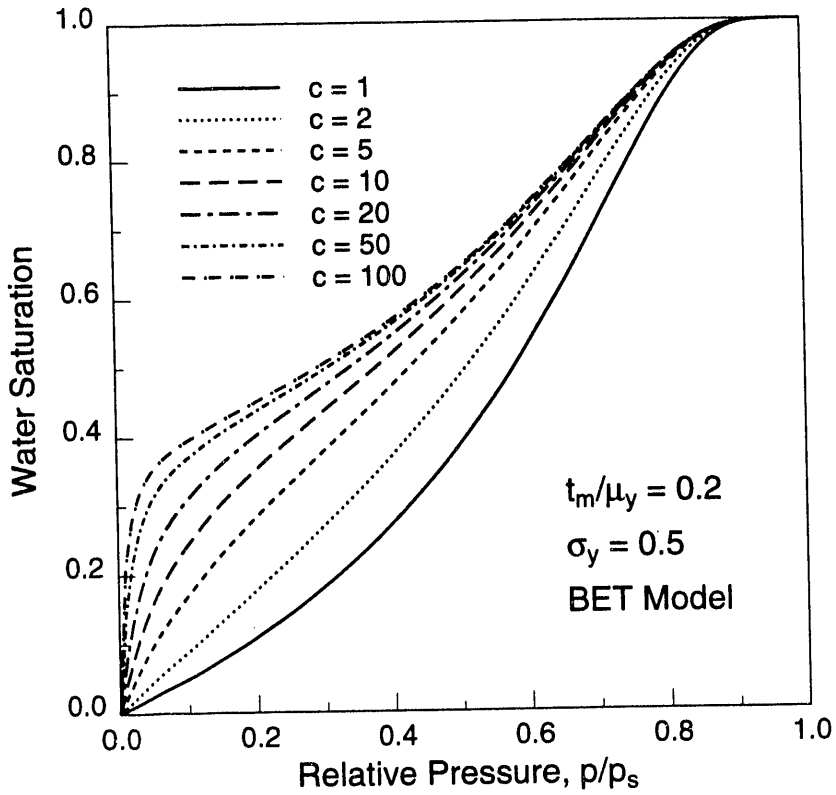

Figure 11: Adsorption in Porous Material - BET Model

2.7 Adsorption and Capillary Condensation

The strategy for developing a model which combines adsorption and capillary condensation is based on the premise that at low relative pressure only adsorption is present. An adsorbed film which thickers as the pressure increases is assumed to be adhered to the walls of spherical pores.

The film thickness t_x may be represented by either Eqs. 24 or 25, depending on the choice of the adsorption model. Adsorption models, other than Langmuir or BET are described in the specialized literature.

In order to have capillary condensation taking place, vapor and adsorbed liquid must be present in the pore. The average radius of a vapor molecule is determined by the pressure and temperature conditions acting upon the molecule, no matter if such a molecule is inside of a pore or present in a continuous vapor phase. Hence, for a vapor molecule to be present in a pore, the inner radius of the absorbed film must be larger than the average radius of a vapor molecule. Of course this has to be viewed as a statistical condition. However, if such a condition is not met, the average mean free path of a vapor molecule in the pore would be less than its mean free path in a

continuous vapor phase. For an isothermal process, this would be equivalent to increasing the pressure acting upon the trapped molecule leading to a non-equilibrium condition with the corresponding continuous vapor phase. Therefore, the average radius of a vapor molecule r_g defines the minimum core radius at which capillary condensation can take place.

When vapor and liquid are present in a pore, the inner radius of the adsorbed film r_m defines the curvature of the vapor-liquid interface. The Kelvin equation establishes a radius of curvature below which the fluid is assumed to be present in the condensate form. Hence, for capillary condensation to materialize into a pore, two conditions on the inner radius of the adsorbed film must be met: 1) it must be less than the radius of curvature predicted by the Kelvin equation, and 2) it must be greater than the average radius of a vapor molecule at corresponding pressure and temperature conditions.

In other words, capillary condensation commences at the pressure and temperature which cause the radius of a vapor molecule to become equal to the radius of curvature of the film inner surface. This is exactly the condition from which Eq. 16 has been derived. Therefore, the relative pressure at which capillary condensation begins when adsorption is present is also defined by Eq. 16. This leads to the important conclusion that such pressure level is not affected by adsorption and, for a given fluid, it depends on temperature only.

In order to construct a combined isotherm we compare the radius of a gas molecule as computed from Eq. 15 to the radius of curvature given by Eq. 6, provided that the same pressure and temperature are used. If $r_g > r_m$ then only adsorption is taking place in the porous material such that Eq. 33 can be used to determine the water saturation at the corresponding pressure.

On the other hand, if $r_g > r_m$ then capillary condensation is a reality. In this case, the lower and upper limits of pore radius defining the capillary condensation region are given by $r_g + t_x$ and $r_m + t_x$, respectively. In this range of pore dimensions, all pores are fully saturated with condensate.

Figure 12 sketches the local water saturation as a function of the pore radius when both adsorption and capillary condensation are present. Eq. 27 has been used to determine the local water saturation due to adsorption for $r > t_x$. Recall that for $r < t_x$ we have that $s_x(r) = 1$. Also, in the region of condensation, $t_x + r_g < r < t_x + t_m$, the local water saturation is unity. Hence, when condensation is present the overall water saturation can be computed by properly substituting the expressions for the local water

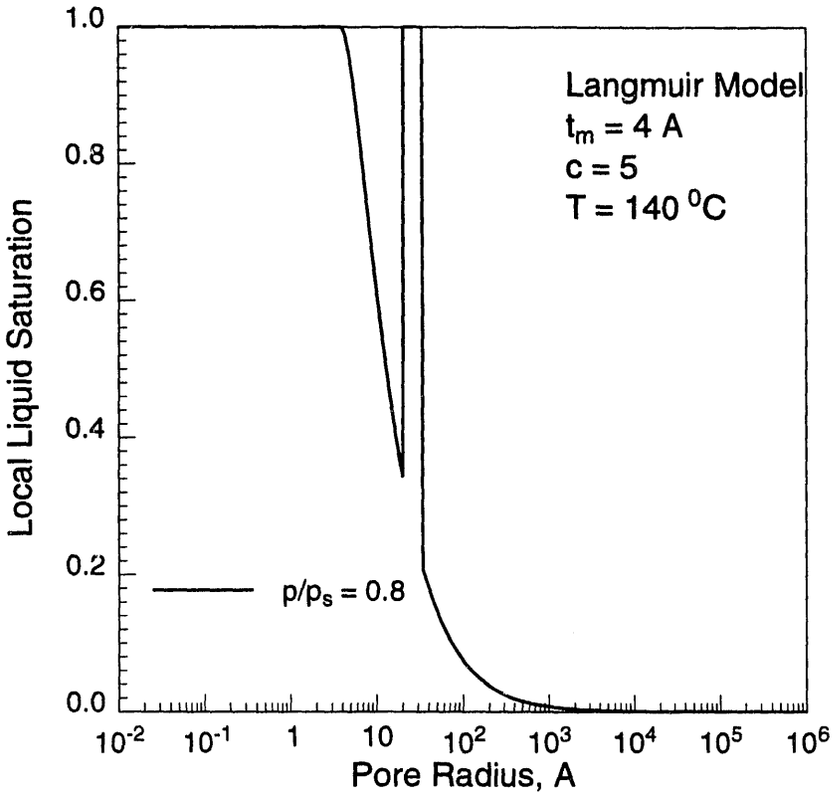

Figure 12: Local Liquid Saturation

saturations into Eq. 29, what results in:

$$S_{wm} = \int_0^{t_x} \lambda(r)\,dr + \int_{t_x}^{t_x+r_g} \frac{t_x}{r}\left(2-\frac{t_x}{r}\right)\lambda(r)\,dr + \int_{t_x+r_g}^{t_x+r_m} \lambda(r)\,dr + \int_{t_x+r_m}^{\infty} \frac{t_x}{r}\left(2-\frac{t_x}{r}\right)\lambda(r)\,dr\,, \qquad r_m > r_g\,. \tag{35}$$

Using the definition of $\mathcal{F}_{x,y}$ given in Eq. 32, then Eq. 35 can be arranged as:

$$S_{wm} = 1 + \mathcal{F}_{x,y}(t_x) - \mathcal{F}_{x,y}(t_x+r_g) + \mathcal{F}_{x,y}(t_x+r_m) - \mathcal{F}_{x,y}(\infty)\,, \qquad r_m > r_g\,. \tag{36}$$

Eq. 33 and 36 may be used to compute the saturation isotherm including the effects of adsorption and capillary condensation. For $r_m < r_g$ only adsorption is relevant, and Eq. 33 shall be used. For $r_m > r_g$, simultaneous adsorption and capillary condensation phenomena can be described by Eq. 36.

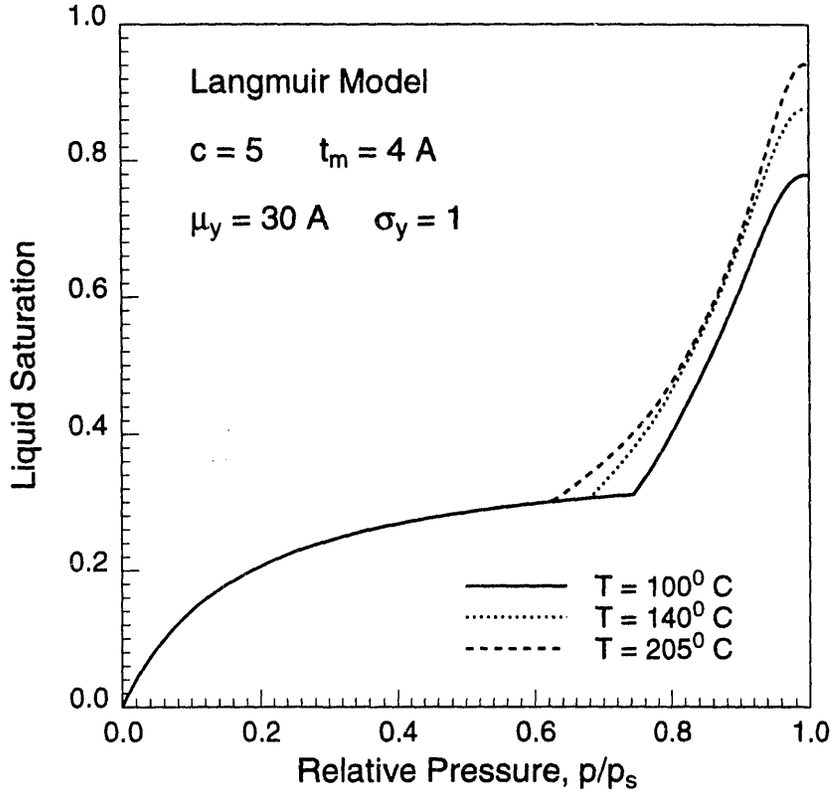

Figure 13: Adsorption and Capillary Condensation Isotherms

Figure 13 displays examples of saturation isotherms computed with a lognormal distribution of pore sizes (μ_y = 20 Å and σ_y = 1) and with the Langmuir model (t_m = 4 Å and c = 5), for temperatures of 100°, 140° and 205°C.

3 ESTIMATION OF ADSORPTION PARAMETERS FROM TRANSIENT EXPERIMENTS

This project is being performed by research assistant Ming Qi, together with Professors Roland N. Horne and Henry J. Ramey, Jr. The goal of the project is to extract adsorption parameters from vapor pressure transient experiments.

The pressure transient experiments continued in the last quarter. Another series of transient pressure tests was run. The purpose of the tests was to double check the repeatability of the transient test equipment, and to improve

the experimental procedure used before so that the runs could be made as close to saturated vapor pressure as possible.

Two different rock samples from the Geysers geothermal field were used and several runs were made using each sample.

The first sample used was the rock sample from the Geysers well OF52-11. The experiment results are shown in Figure 14. Runs 2 and 4 (16ja93.dat and 31ja93.dat) in Figure 14 show good agreement with each other. However, Run 1 (14ja93.dat) started at a much lower relative pressure than Runs 2 and 4. Also, there is a starting pressure difference between Run 3 (23ja93.dat) and Runs 2 and 4.

We thought the main reason for the differences was the instability of the steam temperature. The steam used in the experiments was generated from a steam generator and was introduced via a tube into the oven in which the rock sample holder was placed. The tube is approximately 1.5 feet long. During the run, the steam generator was set at 121°C and the oven, at 125°C. The tube is wrapped with a heated wire and insulation material. The temperature of the tube was maintained at a constant temperature, between 121 - 125°C, by adjusting the voltage applied to the heated wire, the temperature was monitored by a thermocouple.

We used another sample (Geysers shallow reservoir, unknown well) to run the experiment and tried very hard to maintain the steam temperature constant. Seven runs were made and the results are shown in Figure 15. Although some of the results show a good agreement, there were relatively large differences in starting pressure among the runs.

The main reason causing the pressure differences was the temperature. It was difficult to keep the steam temperature constant. This temperature variation was caused mainly by network voltage variations, room temperature changing, and time lag between voltage adjustment and actual heating up of the wire.

Another noticeable phenomenon was the large initial relative pressure difference between the first run of the sample and the following runs. As shown in Figure 15, the first run (11fb93.dat) started at a relative pressure of 0.64 while the fourth run started at 0.78. This kind of difference is also seen in Figure 14 in which the first run (14ja93.dat) started at 0.64 relative pressure and the fourth run (31ja93.dat) started at 0.75. Noticing this phenomenon in Figure 15 (after 4 runs), we conducted another set of runs after the system had been stopped for a relatively long period of time (7 days). Again the

starting pressure difference was obvious although the difference between minimum and maximum starting relative pressure was smaller. This indicated that the differences in starting pressure were not caused only by the system temperature variation, but also by the time elapsed between two consecutive runs. It also suggests that there was some kind of slow reaction taking place between steam and rock.

A new procedure was then used to run the transient experiment in order to achieve higher starting relative pressure as well as to avoid the temperature variation problem. In the new procedure, the internal water reservoir was used as the steam source, in place of the external steam generator. Since both the reservoir and the sample were located inside the oven, they are kept at the same temperature.

Ideally, this would start the experiment at relative pressure of 1. To date, five runs were made and the results are shown in Figure 16.

Observations:

(a) The run indeed started from relative pressures of 1.

(b) The pressure sustained at p/po = 1 for about 1 second and then showed a sudden decrease. In all previous experiments, the pressure began declining immediately after the valve was opened and always showed smooth transient.

(c) Due to the fluctuation of the electricity network, a maximum 0.8 degree variation of the temperature inside the oven existed between different runs.

(d) During the equilibrium period, the bottom pressure output readings of the transducer (in voltage) were greater than its top readings. This was not the case for all previous experiments.

The 0.8 degree temperature drift inside the oven have caused the steam to condense. This condensate may have reevaporated when the pressure decreased during the run. The prolonged pressure response may have been caused by this reevaporation of the condensate, although no liquid was observed at outlet during the experiment.

Noticing the strange behavior of the transducer during the first run (6mr93.dat), we carefully calibrated both top and bottom transducers from 15 psi to atmospheric pressure before the rest of the runs were made. The top readings of the transducer were always higher than the bottom readings over the whole pressure range during calibration. However, in all the following runs, the bottom transducer gave higher readings than the top transducer.

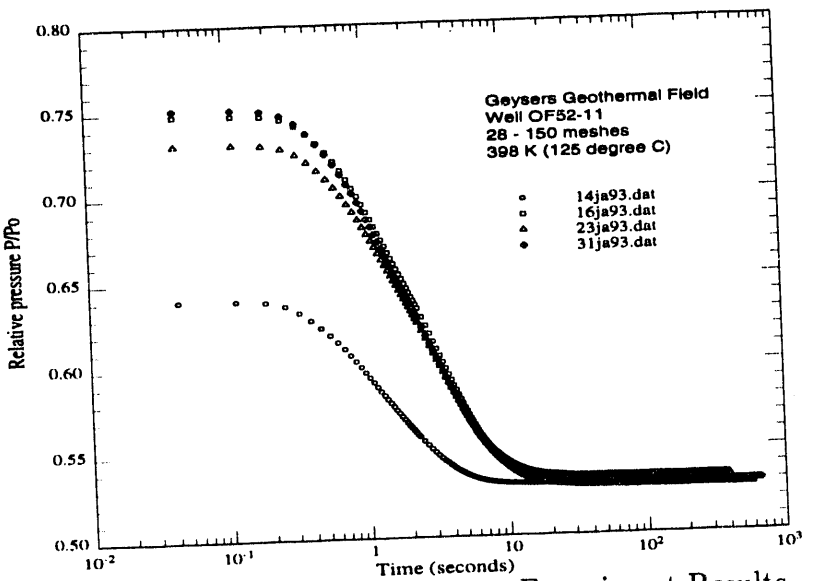

Figure 14: Pressure Transient Experiment Results

This means the transducers were not working properly. The transducers will be replaced and more experiments will be conducted.

4 TRANSIENT ADSORPTION EXPERIMENT - SALINITY AND NONCONDENSIBLE GAS EFFECTS

This project is being conducted by Research Assistant, Steve Palar, and Professsors Roland N. Horne and Henry J. Ramey, Jr. The purpose of this project is to analyze the adsorption and desorption of superheated steam in geothermal core materials.

4.1 Introduction

Modeling of steam flow in porous medium has been undertaken in the past. *Herkelrath et al.* (1983) designed the current equipment, used for the sorption

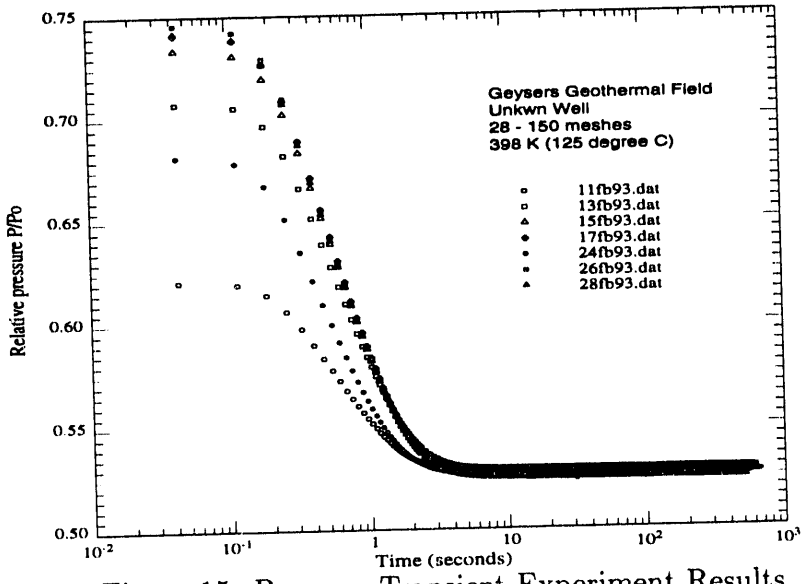

Figure 15: Pressure Transient Experiment Results

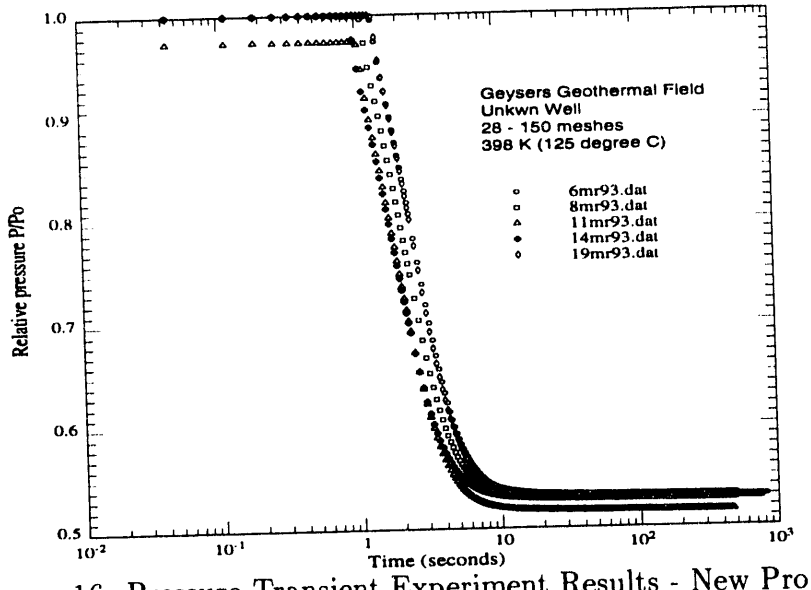

Figure 16: Pressure Transient Experiment Results - New Procedure

experiment. The result of their experiment concluded that adsorption caused a delay in the steam pressure breakthrough. Their work will be used as a basis for further investigation of sorption in the porous medium.

In an earlier study at Stanford, Harr (1991) experimented with transient flow of superheated steam. He applied a one-dimensional steam flow simulator by *Nghiem and Ramey* (1991) to his data. This project will use the same model, although modification to the model may be necessary.

4.2 Discussion on the Equipment

Last quarter was spent familiarizing with the equipment and the run procedure. Some adjustments to the equipment are necessary to best meet the objective of the experiment.

The proposed tentative adjustments are to:

- Elongate the sample holder. By extending the length, the desorption time will be longer and the bottom transducer will be closer to the bottom of the sample. However the drawback is the requirement for a substantial volume of sample, which we are in the process of obtaining.

- Reinstall the valve system for the nitrogen gas chamber inside the air-bath. The defective valve was removed previously. Noncondensable gas such as nitrogen and carbon dioxide will be used to compare results with the steam flow.

4.3 Next Work

Currently efforts are geared up to run superheated steam and to compare the result with a separate run of nitrogen. Further work will be contingent upon those data. Changes of the procedure and adjustments to the equipment configuration might be possible.

More samples from the Geysers are needed to fill the proposed longer sample holder.

5 THE PHYSICS OF INJECTION OF WATER INTO, TRANSPORT AND STORAGE OF FLUIDS WITHIN, AND PRODUCTION OF VAPOR FROM GEOTHERMAL RESERVOIRS

This project is under the direction of Research Assistant, John W. Hornbrook and Professor Roland N. Horne. The goal of this work is to better understand the physics of fluid storage and transport in geothermal reservoirs with adsorption effects present. In particular, this research is aimed at determining whether or not adsorption significantly affects the transport of fluid and heat in geothermal reservoirs during reinjection.

5.1 Introduction

The effects of adsorption on the pressure response in geothermal reservoirs must be fully understood to effectively design injection and production programs. It is the purpose of this research to isolate the effects of adsorption on the flow of fluids in geothermal reservoirs during reinjection and to determine if these effects are significant.

The research focuses on three flow regions associated with an injection/production pair in a geothermal reservoir. The three regions are near injector flow, boiling front flow, and near producer flow. These three regions correspond to, respectively, single phase flow of water, simultaneous flow of water and vapor, and single phase flow of vapor. In order to understand the role of adsorption in fluid transport through porous media, adsorption effects must be fully characterized in each of the three flow regions.

The goal of the current research is to derive analytical expressions that describe the flow of fluids in geothermal reservoirs with adsorption effects included. At this stage, analytical solutions have been obtained for the two single phase flow regions described above and work is continuing in the multiphase flow region.

Single Phase Regions

A perturbation expansion solution in terms of Green's functions has been derived which describes the flow of fluids in the single phase regions. The first term in the expansion describes pressure decline without adsorption effects while subsequent terms introduce the effects of adsorption on the pressure response. Thus, the solution isolates the effects of adsorption so its effects may be studied. The perturbation derivation was included in the Winter, 1993 Quarterly Report.

Multiphase Region

In the multiphase region, the effects of adsorption become much more complicated. Instead of simply altering pressure decline, adsorption may also affect the temperature, width, and speed of the boiling front. In order to isolate the effects of adsorption, a one-dimensional, fully-implicit simulator is being written which will be used to track the boiling front under various conditions. The simulator is being constructed without the assumption of thermal or thermodynamic equilibrium so the full effects of adsorption may be determined. Additionally, the simulator results, along with the analytical equations described above, will be used to study adsorption effects in the single phase flow regions.

6 INJECTION OPTIMIZATION AT THE GEYSERS GEOTHERMAL FIELD

This work is being performed by Research Assistant, Zosimo Aunzo under the guidance of Professor Roland N. Horne.

6.1 Previous Work

During the last nuarter, work involved mostly literature survey and data acquisition. An extensive database management on the Geysers up to 1989 was done at the Lawrence Berkeley Laboratory. This report was used as the main reference for the available data. The actual data were taken from the

Division of Oil and Gas, Department of Conservation in Santa Rosa. The data available to us right now are the open file wells.

6.2 Future Work

We will start analyzing the general trends by looking at the production history of the wells per lease. Then we will attempt to correlate this with the injection done in the area and try to determine the effect of injection. Once we obtain correlation between injection-production sectors, we will look in detail at the response and quantify the effect of injection.

7 A MODEL TO TEST MULTIWELL DATA INTERPRETATION FOR HETEROGENEOUS RESERVOIRS

This investigation is performed by Research Assistant, Xianfa Deng, and Professor Roland N. Horne. The purpose is to develop an interpretation scheme for multiwell data.

7.1 A Two-Dimensional Model

Consider a closed rectangle reservoir with mobility and storativity as functions of one direction only, its Green's function satisfies

$$\frac{\partial}{\partial x}[(ax+b)\frac{\partial G}{\partial x}]+\frac{\partial}{\partial y}[(ax+b)\frac{\partial G}{\partial y}]=(ax+b)\frac{\partial G}{\partial t} \tag{37}$$

which, after transformation with any constant c,

$$\begin{cases} x' = ax+b \\ y' = ay+c \\ t' = a^2 t \end{cases} \tag{38}$$

is equivalent to the following problem:

$$\frac{1}{x}\frac{\partial}{\partial x}(x\frac{\partial G}{\partial x})+\frac{\partial^2 G}{\partial y^2}=\frac{\partial G}{\partial t} \tag{39}$$

with $0 \leq a \leq x \leq b$ and $0 \leq y \leq l$.

$$G(x,x',y,y',0) = \frac{\delta(x-x')\delta(y-y')}{x'} \tag{40}$$

Let $G(x,x',y,y',t) = G_1(x,x',t)G_2(y,y',t)$, then this two-dimension problem can be decomposed into two one-dimensional problems, $G(x,x',y,y',t) = G_1(x,x',t)G_2(y,y',t)$

$$\frac{1}{x}\frac{\partial}{\partial x}(x\frac{\partial G_1}{\partial x}) = \frac{\partial G_1}{\partial t} \tag{41}$$

with $0 \leq a \leq x \leq b$ and $G_1(x,x',0) = \frac{\delta(x-x')}{x'}$.

$$\frac{\partial^2 G_2}{\partial y^2} = \frac{\partial G_2}{\partial t} \tag{42}$$

with $0 \leq y \leq l$ and $G_2(y,y',0) = \delta(y-y')$. This is one dimension homogeneous reservoir with a Green's function (*Gringarten [1973]*) as

$$G_2(y,y',t) = \frac{1}{l}(1 + 2\sum_{n=1}^{\infty} e^{-\frac{n^2\pi^2 t}{l^2}} cos\frac{n\pi y}{l} cos\frac{n\pi y'}{l}). \tag{43}$$

To obtain $G_1(x,x',t)$, we try the method of separating variables by assuming

$$G_1 = X(x)T(t) \tag{44}$$

resulting in two equations. The first one is

$$T' + \alpha^2 T = 0 \tag{45}$$

which has solution $T(t) = be^{-\alpha^2 t}$.

The second equation is

$$X'' + \frac{X'}{x} + \alpha^2 X = 0 \tag{46}$$

which is a Bessel equation with general solution:

$$X(x) = c_1 J_0(\alpha x) + c_2 Y_0(\alpha x) \tag{47}$$

Applying boundary conditions,

$$\begin{cases} c_1 J_1(a\alpha) + c_2 Y_1(a\alpha) = 0 \\ c_1 J_1(b\alpha) + c_2 Y_1(b\alpha) = 0 \end{cases} \tag{48}$$

and denoting α_n, $n = 1, 2, ...$ as the roots of

$$J_1(a\alpha)Y_1(b\alpha) - J_1(b\alpha)Y_1(a\alpha) = 0 \tag{49}$$

then

$$X_n(x) = C_n[J_1(a\alpha_n)Y_0(\alpha_n x) - J_0(\alpha_n x)Y_1(a\alpha_n)] \tag{50}$$

and the eigenfunctions are

$$G_{1n}(x,t) = C_n e^{-\alpha_n^2 t}[J_1(a\alpha_n)Y_0(\alpha_n x) - J_0(\alpha_n x)Y_1(a\alpha_n)] \tag{51}$$

Thus the Green's function is

$$G_1(x,t) = \sum_{n=1}^{\infty} C_n e^{-\alpha_n^2 t}[J_1(a\alpha_n)Y_0(\alpha_n x) - J_0(\alpha_n x)Y_1(a\alpha_n)] \tag{52}$$

where C_n are decided by initial condition

$$\delta(x - x') = x' \sum_{n=1}^{\infty} C_n[J_1(a\alpha_n)Y_0(\alpha_n x) - J_0(\alpha_n x)Y_1(a\alpha_n)] \tag{53}$$

We can obtain C_n by using orthogonality of

$$y_n = J_1(a\alpha_n)Y_0(\alpha_n x) - J_0(\alpha_n x)Y_1(a\alpha_n) \tag{54}$$

$$\int_a^b x y_n(x) y_m(x) dx = 0 \qquad m \neq n \tag{55}$$

Multiplying $xy_m(x)$ on both sides of Eqn. 53 and integrating on (a, b), we have

$$C_n = \frac{\int_a^b x y_n(x)\delta(x - x')dx}{x' \int_a^b x y_n^2(x)dx} = \frac{y_n(x')}{\int_a^b x y_n^2(x)dx} \tag{56}$$

and

$$G_1(x,t) = \sum_{n=1}^{\infty} \frac{y_n(x')y_n(x)}{\int_a^b x y_n^2(x)dx} e^{-\alpha_n^2 t} \tag{57}$$

Therefore the Green's function is

$$G(x,x',y,y',t) = \frac{1}{l}(1 + 2\sum_{n=1}^{\infty} e^{-\frac{n^2\pi^2 t}{l^2}} cos\frac{n\pi y'}{l} cos\frac{n\pi y}{l})$$

$$\sum_{n=1}^{\infty} \frac{[J_1(\alpha_n a)Y_0(\alpha_n x') - Y_1(\alpha_n a)J_0(\alpha_n x')][J_1(\alpha_n a)Y_0(\alpha_n x) - Y_1(\alpha_n a)J_0(\alpha_n x)]}{e^{\alpha_n^2 t}\int_a^b x[J_1(\alpha_n a)Y_0(\alpha_n x) - Y_1(\alpha_n a)J_0(\alpha_n x)]^2 dx} \tag{58}$$

where α_n $(n = 1, 2, 3, ...)$ are roots of

$$J_1(\alpha_n a)Y_1(\alpha_n b) - Y_1(\alpha_n a)J_1(\alpha_n b) = 0 \tag{59}$$

If we have one active well with production rate $q(t)$ at position (x', y'), then the pressure response at place (x, y) is

$$p_i - p(x, y, t) = \int_0^t \frac{q(\tau)}{\pi r_w^2 h} G(x, x', y, y', t - \tau)d\tau \tag{60}$$

With this two-dimensional model with continuous variation of mobility and storativity, we can generate multiwell pressure data and test any interpretation scheme for heterogeneous reservoirs. The general flow equation in a two-dimensional heterogeneous reservoir is

$$\frac{\partial}{\partial x}\frac{k(x,y)}{\mu(x,y)}\frac{\partial G}{\partial x} + \frac{\partial}{\partial y}\frac{k(x,y)}{\mu(x,y)}\frac{\partial G}{\partial y} = \phi(x,y)c_t(x,y)\frac{\partial G}{\partial t} \tag{61}$$

One scheme on our investigating schedule for two dimensional heterogeneous reservoir will be as follows:

- From the pressure data measured at multiple wells, generate pressure distributions at various time on the whole region by interpolation scheme such as kringing.
- Once the pressure as a function of x, y, t is known, Eq. 61 is a first order partial differential equation for $\frac{k(x,y)}{\mu(x,y)}$. This equation can be solved by numerical methods to obtain $\frac{k(x,y)}{\mu(x,y)}$.

The restrictions of this interpretation scheme are:

- It is invalid for three-dimensional problems because the pressures are not available for different locations at vertical direction.
- Pressure data from multiple observation wells at different locations are needed in order to make spatial interpolation possible.

7.2 Nomenclature

a, b = range of reservoir in x direction
c_t = compressibility
G = Green's function
h = thickness
J, Y = Bessel functions
k = permeability
l = length of reservoir in y direction
p = pressure
p_i = initial pressure
q = flow rate
r_w = wellbore radius of active well
t = time
x, y = coordinate for observation well in Cartesian system
x', y' = coordinate for source well in Cartesian system
α_n = roots of equation
δ = Dirac function
μ = viscosity
τ = time integral variable
ϕ = porosity

8 EARTH TIDE EFFECTS ON DOWNHOLE PRESSURE MEASUREMENTS.

This project is being undertaken by Research Assistant Edgar Dias under the guidance of Professor Henry J. Ramey, Jr. The aim of the project is to understand the relationship between earth-tide forces, and the pressure response to these changes measured downhole in oil reservoirs.

8.1 Work to Date

In the last two reports on this project, we covered a review of the existing research done on this subject, and we derived a governing equation which

included the contribution of the volume strain of the rock structure due to earth tides, to the existing diffusivity equation.

8.2 Aim of the Project

In this report, we use a one-dimensional simulation of a laboratory model that represents a reservoir subject to a sinusoidal pressure disturbance, and we derive an expression for the response expected. We use a core to represent the reservoir. One end of the core is connected hydraulically with a volume of fluid. This represents the wellbore and we will refer to it as the *bore volume.*

We consider two cases. In the first case, a sinusoidal pressure signal is imposed at one end. We derive the pressure response in the bore volume. This is similar to a case where earth-tide effects are coupled to a reservoir via a supporting aquifer. In the second case, one end of the core is sealed, and the confining pressure on the core is oscillated sinusoidally. This is similar to an earth-tide disturbance coupled to a sealed reservoir, via the overlying formation. We derive the expected pressure response in the bore volume communicating with the fluid in the pores.

CASE I

We start with a core of length L, connected with the bore volume V_2. The other end is connected to a sinusoidal pressure input, oscillating with frequency w. This is similar to the case where a reservoir is in communication with an aquifer that transmits the earth-tide excitation forces.

8.3 Mathematical Derivation

We have the governing equation for fluid flow:

$$(\frac{k}{\mu\beta\phi})\nabla^2 p = \frac{\partial p}{\partial t} \tag{62}$$

Letting $a^2 = \frac{k}{\mu\beta\phi}$, we obtain:

$$a^2\frac{\partial^2 p}{\partial x^2} = \frac{\partial p}{\partial t} \tag{63}$$

with the boundary conditions:
at $x = 0$,

$$p = p_1 \cos wt \tag{64}$$

and at $x = L$

$$\frac{\partial p}{\partial t} = (\frac{kA}{\mu\beta V_2})\frac{\partial p}{\partial x} \tag{65}$$

Letting $C = \frac{kA}{\mu\beta V_2}$ then,

$$\frac{\partial p}{\partial t} = C\frac{\partial p}{\partial x} \tag{66}$$

where:
k = permeability of the core (md)
μ = fluid viscosity (cp)
ϕ = core porosity (fraction)
β = fluid compressibility (psi^-1)
A = core cross sectional area (m^2)
w = frequency of oscillation(cyc/sec).

Let the steady state solution $P_s = X(x)e^{iwt}$, then substituting in Eq. 62, we obtain after differentiating:

$$a^2 X'' e^{iwt} = iwXe^{iwt} \tag{67}$$

$$X'' + (\frac{-i\omega}{a^2})X = 0 \tag{68}$$

Letting $\beta^2 = \frac{-i\omega}{a^2}$, then $\beta = \sqrt{\frac{w}{2a^2}}(1-i) = \alpha(1-i)$, where $\alpha = \sqrt{\frac{w}{2a^2}}$.

The general solution to this equation is:

$$P_s = (A\cos\beta x + B\sin\beta x)e^{iwt} \tag{69}$$

Substituting this in the boundary condition at $x = 0$ we obtain:

$$p = p_1 \cos wt = p_1 e^{iwt} \tag{70}$$

then:

$$Ae^{iwt} = p_1 e^{iwt} \tag{71}$$

$$A = p_1 \tag{72}$$

$$P_s = (p_1 \cos \beta x + B \sin \beta x) e^{iwt} \tag{73}$$

Now,

$$\frac{\partial P_s}{\partial t} = iw(p_1 \cos \beta x + B \sin \beta x) e^{iwt} \tag{74}$$

$$\frac{\partial P_s}{\partial x} = \beta(-p_1 \sin \beta x + B \cos \beta x) e^{iwt} \tag{75}$$

and substituting these into the boundary conditions at $x = L$, we obtain:

$$\frac{\partial P_s}{\partial t} = C \frac{\partial P_s}{\partial x} \tag{76}$$

$$iw(p_1 \cos \beta L + B \sin \beta L) = C\beta(B \cos \beta L - p_1 \sin \beta L) \tag{77}$$

$$B(C\beta \cos \beta L - iw \sin \beta L) = p_1(iw \cos \beta L + C\beta \sin \beta L) \tag{78}$$

$$B = \frac{p_1(C\beta \sin \beta L + iw \cos \beta L)}{(C\beta \cos \beta L - iw \sin \beta L)} \tag{79}$$

$$= \frac{p_1(\frac{\sin 2\beta l}{2}(\beta^2 - w^2) + iw\beta)}{(\beta^2 \cos^2 \beta L + w^2 \sin^2 \beta L)} \tag{80}$$

So a general form of solution is:

$$P_s = (p_1 \cos \beta x + B \sin \beta x) e^{iwt} \tag{81}$$

where,

$$B = \frac{p_1(\frac{\sin 2\beta l}{2}(\beta^2 - w^2) + iw\beta)}{(\beta^2 \cos^2 \beta L + w^2 \sin^2 \beta L)} \tag{82}$$

Using the relationships,

$$\sin \beta L = \sin \alpha L \cos \alpha Li - \cos \alpha L \sin \alpha Li \tag{83}$$

$$\cos \beta L = \cos \alpha L \cos \alpha Li + \sin \alpha L \sin \alpha Li \tag{84}$$

$$\sin \alpha Li = \frac{i}{2}(e^{\alpha L} - e^{-\alpha L}) \tag{85}$$

$$\cos \alpha Li = \frac{1}{2}(e^{\alpha L} + e^{-\alpha L}) \tag{86}$$

we can substitute in the above expression to obtain,

$$Re(P_s) = p_1\sqrt{R_1^2+R_2^2}\left(\frac{R_1}{\sqrt{R_1^2+R_2^2}}\cos wt - \frac{R_2}{\sqrt{R_1^2+R_2^2}}\sin wt\right) \quad (87)$$

where,

$$R_1 = M + N \quad (88)$$

$$M = \frac{(e^{\alpha x}+e^{-\alpha x})}{2}\{\cos\alpha x + \frac{\sin\alpha x}{Z}\{\frac{\sin 2\alpha L}{2}(2(C\alpha)^2 - w^2) - \cos 2\alpha L(wC\alpha)\}\} \quad (89)$$

$$N = \frac{(e^{\alpha x}-e^{-\alpha x})}{2Z}\cos\alpha x\{\frac{(e^{2\alpha L}+e^{-2\alpha L})}{2}(wC\alpha) - \frac{(e^{2\alpha L}-e^{-2\alpha L})}{4}(w^2+2(C\alpha)^2\} \quad (90)$$

$$R_2 = S + T \quad (91)$$

$$S = \frac{(e^{\alpha x}-e^{-\alpha x})}{2}\{\sin\alpha x - \frac{\cos\alpha x}{Z}\{\frac{\sin 2\alpha L}{2}(2(C\alpha)^2 - w^2) - \cos 2\alpha L(wC\alpha)\}\} \quad (92)$$

$$T = \frac{(e^{\alpha x}+e^{-\alpha x}}{2Z}\sin\alpha x\{\frac{(e^{2\alpha L}+e^{-2\alpha L})}{2}(wC\alpha) - \frac{(e^{2\alpha L}-e^{-2\alpha L})}{4}(w^2+2(C\alpha)^2)\} \quad (93)$$

and

$$Z = \frac{(e^{2\alpha L}+e^{-2\alpha L})}{4}(2(C\alpha)^2 + w^2) + \frac{(2(C\alpha)^2 - w^2)}{2}\cos 2\alpha L$$

$$- \frac{(wC\alpha)}{2}(e^{2\alpha L} - e^{-2\alpha L}) + (wC\alpha)\sin 2\alpha L \quad (94)$$

Thus we can write the steady state response as:

$$Re(P_s) = Ampl(\cos wt + \psi) \quad (95)$$

where,

$$Ampl = p_1(\sqrt{R_1^2+R_2^2}) \quad (96)$$

and

$$\tan\psi = \frac{R_2}{R_1} \quad (97)$$

give the amplitude and the phase-shift of the response signal.

8.4 Response Analysis

In order to analyze the responses one may expect in a typical experiment, we used the following values for the parameters involved.
Diameter (d) of the core = 0.05 m
Length(L) of the core = 0.10 m
Porosity $\phi = .01$
Fluid saturating the core: water at 70 degF.
Fluid Viscosity $\mu = 10.0$ cp
Fluid Compressibility $comp = 10^-6(psi^-1)$
Permeability of the core $k = 100md$
Oscillation frequency $w = 0.01\ cycles/sec$

A program was written to calculate the response for variations in different parameters. Several parameters were varied one at a time, keeping the others at the above fixed values, assuming isothermal conditions.

In all the following plots the response is characterized by phase-shift (deg), and amplitude ratio $Ampl/P_1$.

Since we are primarily interested in response in the bore volume, where such measurements are feasible, we plotted the response at $X/L = 1.0$, while varying parameters. We varied all the parameters and found that the response could be normalized by plotting phase-shifts and amplitude ratios against wD where $wD = (comp\ w\ \mu\ bore\ vol)/(core\ vol\ k\ 10^-9)$, as shown in Fig. 17. The phase shifts and amplitude responses vary for different values of wD, and this reponse may be large or small depending on the relationship between the parameters, as given by wD. In general phase shift decreases as k increase and the amplitudes show consistent increase with increasing k over values of practical interest. As the bore volume decreases, the phase shifts decrease to zero, while the amplitudes increase to unity. Phase shift tends to a maximum value for certain values of oscillation frequency, as noted earlier by Arditty et al (1978), however amplitudes decrease consistently as frequency increase from a threshold value. Compressibility and viscosity affect the response in the same way, namely an increase in either leads to an increase in the phase shift and a decrease in the amplitude ratio. We note a threshold value below which the response is negligible. This threshold is dependent on frequency among other factors as noted by Bredehoeft (1967).

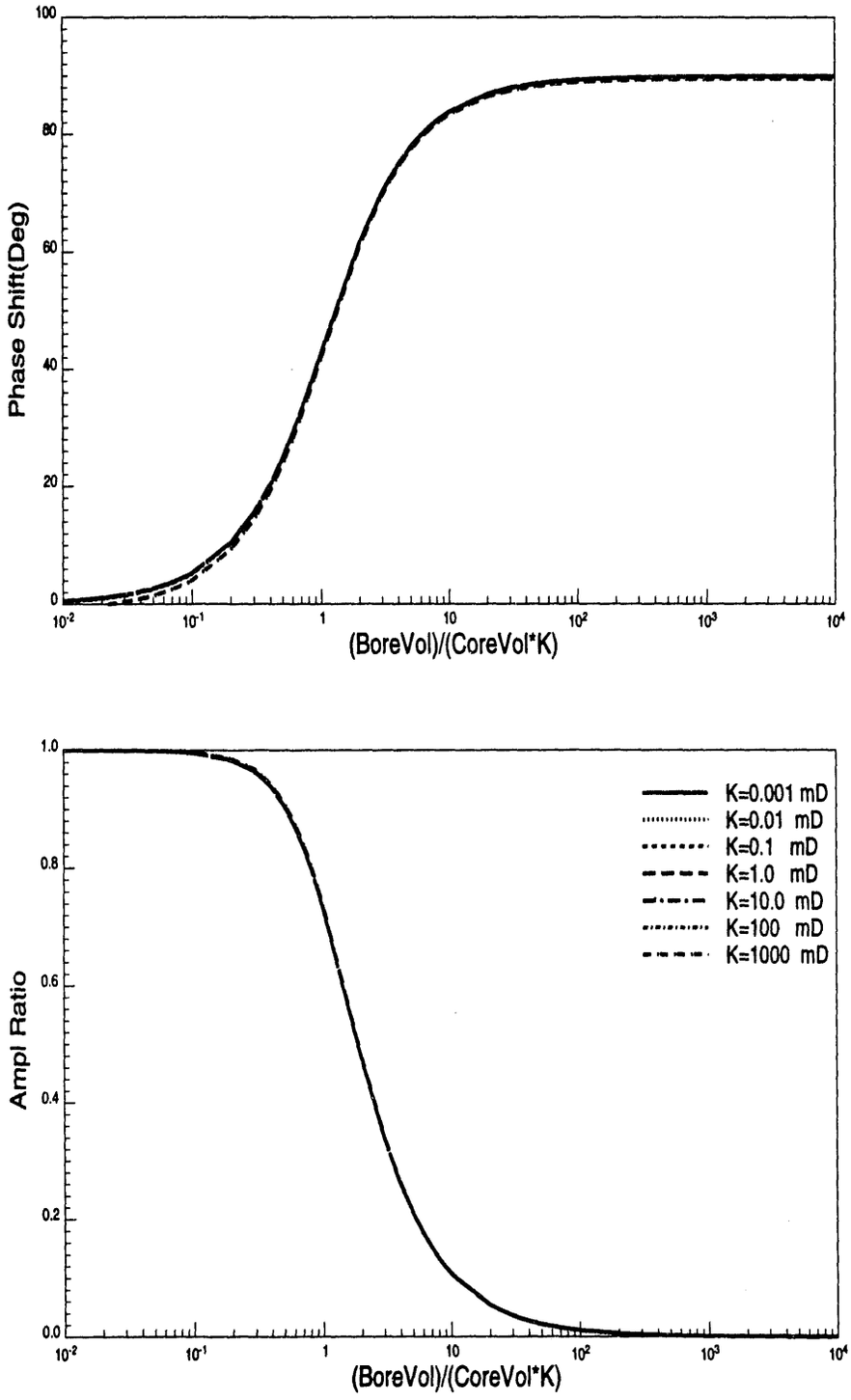

Figure 17: Case I: Response vs. normalized factor wD

CASE II

Here we analyze another experiment. The core is connected to a bore volume, as stated earlier. One end of the core is sealed, and a confining pressure applied to the core is oscillated sinusoidally. We derive the expression for the pressure response in the bore volume. This case can be compared to a sealed reservoir, penetrated by a well. The earth-tide exciting forces are coupled to the reservoir by the adjacent impermeable boundaries and the overlying strata.

8.5 Mathematical Derivation

Let a denote grain matrix, and let b denote fluid in the reservoir. Then from mass balance:

$$\frac{\partial}{\partial t}\{(1-\phi)\rho_a\} + div\{(1-\phi)\rho_a v_a\} = 0 \tag{98}$$

$$\frac{\partial}{\partial t}\{\phi\rho_b\} + div\{\rho_b\phi v_b\} = 0 \tag{99}$$

where, ρ_a is the grain density, ρ_b is the fluid density, v_b is the fluid velocity and v_a is the grain velocity. Thus we have

$$q_a = (1-\phi)v_a \tag{100}$$

$$q_b = (1-\phi)v_b \tag{101}$$

where ϕ is the porosity and q_a and q_b are flow rates of grain and fluid respectively.

Now we know that:

$$q = \frac{-k_p\rho_b g}{\mu}\nabla\theta = \phi(v_b - v_a) \tag{102}$$

where:
θ = flow potential
k_p = core permeability
μ = fluid viscosity
g = gravitational acceleration

We can express flow potential as:

$$\theta = \int_{z_o}^{z} \partial z + \int_{p_0}^{p} \frac{\partial p}{\rho_b g} \tag{103}$$

Also, compressibility β, can be expressed as:

$$\beta = \frac{\partial \rho_b}{\rho_b \partial p} \tag{104}$$

Now expanding Eq. 98, we obtain:

$$\frac{\partial \phi}{\partial t} = (1-\phi) div(v_a) - v_a grad(\phi) \tag{105}$$

and from Eq. 99 we derive:

$$\phi \frac{\partial \rho_b}{\partial t} + \rho_b \frac{\partial \phi}{\partial t} + \rho_b \phi div(v_b) + v_b grad(\rho_b \phi) = 0 \tag{106}$$

differentiating Eq. 103 we have:

$$\rho_b g \nabla^2 \theta = \nabla^2 p - \beta gradp.gradp \tag{107}$$

and substituting in Eq. 102 we obtain:

$$\frac{-k_p \rho_b g}{\mu} \nabla^2 \theta = \phi div(v_b - v_a) + (v_b - v_a) grad\phi \tag{108}$$

Now, substituting for $\nabla^2 \theta$ from Eq. 107 we obtain:

$$\frac{-k_p}{\mu}(\nabla^2 p - \beta gradp.gradp) = \phi div(v_b - v_a) + (v_b - v_a) grad\phi \tag{109}$$

Expanding this:

$$\frac{-k_p}{\mu} \nabla^2 p = \phi div(v_b - v_a) + (v_b - v_a) grad\phi - \frac{k_p \beta}{\mu} gradp.gradp \tag{110}$$

$$= (v_b - v_a) grad\phi + \phi div(v_b) - \phi div(v_a) - \frac{k_p \beta}{\mu} gradp.gradp \tag{111}$$

Substituting for expression $div(v_b)$ from Eq. 106 we obtain:

$$= (v_b - v_a)grad\phi + \frac{1}{\rho_b}\{-\phi\frac{\partial\rho_b}{\partial t} - \rho_b\frac{\partial\phi}{\partial t} - v_b grad(\rho_b\phi)\} - \phi div(v_a) - \frac{k_p\beta}{\mu} gradp.gradp \tag{112}$$

$$= (v_b - v_a)grad\phi - \frac{\phi}{\rho_b}\frac{\partial\rho_b}{\partial t} - \frac{\partial\phi}{\partial t} - v_b grad\phi - \phi div(v_a) - \frac{k_p\beta}{\mu} gradp.gradp \tag{113}$$

$$= -\frac{\phi}{\rho_b}\frac{\partial\rho_b}{\partial t} - \frac{v_b}{\rho_b}\phi grad(\rho_b) - \{-\frac{\partial\phi}{\partial t} - v_a grad\phi - \phi div(v_a)\} - \frac{k_p\beta}{\mu} gradp.gradp \tag{114}$$

and ignoring inertial terms and second order terms and using the relationship,

$$-\frac{1}{\rho_b}\frac{\partial\rho_b}{\partial t} = -\beta\frac{\partial p}{\partial t} \tag{115}$$

$$= -\phi\beta\frac{\partial p}{\partial t} - div(v_a) \tag{116}$$

then we have,

$$\frac{k_p}{\mu}\nabla^2 p = \phi\beta\frac{\partial p}{\partial t} + div(v_a) \tag{117}$$

$$= \phi\beta\frac{\partial p}{\partial t} + \frac{\partial e}{\partial t} \tag{118}$$

where e is the matrix strain, $e = div(u_a)$ where u_a is the matrix displacement

$$\partial\sigma = K_b\partial e - \alpha\partial p \tag{119}$$

Now we know, $\alpha = (1 - \frac{K_b}{k_s})$, where K_b is the bulk modulus and K_s is the matrix grain modulus, so:

$$\frac{\partial e}{\partial t} = \frac{1}{K_b}\frac{\partial\sigma}{\partial t} + \frac{\alpha}{K_b}\frac{\partial p}{\partial t} \tag{120}$$

and substituting this we arrive at a governing equation for our new conditions,

$$\frac{k_p}{\mu}\nabla^2 p = \phi\beta\frac{\partial p}{\partial t} + \frac{1}{K_b}\frac{\partial\sigma}{\partial t} + \frac{\alpha}{K_b}\frac{\partial p}{\partial t} \tag{121}$$

$$= \frac{1}{K_b}\frac{\partial\sigma}{\partial t} + \{\phi\beta + \frac{\alpha}{K_b}\}\frac{\partial p}{\partial t} \tag{122}$$

We now consider the following boundary conditions: at $x = 0$, we have $\frac{\partial p}{\partial x} = 0$, due to the sealing boundary, and at $x = L$:

$$\frac{\partial p}{\partial t} = \frac{k_p A}{\mu \beta V_2} \frac{\partial p}{\partial x} = C \frac{\partial p}{\partial x} \tag{123}$$

where $C = \frac{k_p A}{\mu \beta V_2}$ the terms are as defined in Case I.

We model the oscillating confining pressure as follows. We know $\sigma = -p_c$, where p_c is the confining pressure so we express the confining pressure as:

$$\sigma = -p_c e^{iwt} \tag{124}$$

Substituting this in the governing equation,

$$\frac{k_p}{\mu} \frac{\partial^2 p}{\partial x^2} = -\frac{iw}{K_b} p_c e^{iwt} + \{\phi\beta + \frac{\alpha}{K_b}\} \frac{\partial p}{\partial t} \tag{125}$$

The steady state solution is:

$$P_s = X(x) e^{iwt} \tag{126}$$

Thus, we have:

$$\frac{k_p}{\mu} X'' - iw\{\phi\beta + \frac{\alpha}{K_b}\} X + \frac{iw}{K_b} p_c = 0 \tag{127}$$

Let $O = \frac{k_p}{\mu} iM = iw\{\phi\beta + \frac{\alpha}{K_b}\}$ and $iN = \frac{iwp_c}{K_b}$ then:

$$OX'' - iMX + iN = 0 \tag{128}$$

Letting $Q^2 = \frac{M}{O}$, then we have a general solution:

$$X(x) = C_1 e^{\sqrt{i}Qx} + C_2 e^{-\sqrt{i}Qx} + \frac{N}{M} \tag{129}$$

and,

$$P_s = X(x) e^{iwt} \tag{130}$$

Now let $R = \frac{N}{M}$ and we can solve by substituting this general equation in the boundary conditions:

$$P_s = R\frac{\{iw(e^{\sqrt{i}Qx} + e^{-\sqrt{i}Qx}) + (e^{\sqrt{i}QL} - e^{-\sqrt{i}QL})C\sqrt{i}Q - iw(e^{\sqrt{i}QL} + e^{-\sqrt{i}QL})\}}{\{(e^{\sqrt{i}QL} - e^{-\sqrt{i}QL})C\sqrt{i}Q - iw(e^{\sqrt{i}QL} + e^{-\sqrt{i}QL})\}}e^{iwt} \tag{131}$$

We can expand this expression and separate terms to obtain:

$$Re(P_s) = Ampl\{\cos(wt + \psi)\} \tag{132}$$

where,

$$\tan\psi = \frac{(Z(Y+J) - Y(Z-K))}{(Z(Z-K) + Y(Y+J))} \tag{133}$$

and

$$Ampl = \frac{R}{(Z^2+Y^2)}\sqrt{\{\{Z(Z-K) + Y(Y+J)\}^2 + \{Z(Y+J) - Y(Z-K)\}^2\}} \tag{134}$$

where $\frac{QL}{\sqrt{2}} = ql$

$$Z = \{(e^{ql} - e^{-ql})(\frac{CQ}{\sqrt{2}}\cos ql + w\sin ql) - (e^{ql} + e^{-ql})\frac{CQ}{\sqrt{2}}\sin ql\} \tag{135}$$

$$Y = \{(e^{ql} - e^{-ql})\frac{CQ}{\sqrt{2}}\cos ql + (e^{ql} + e^{-ql})(\frac{CQ}{\sqrt{2}}\sin ql - w\cos ql)\} \tag{136}$$

Let $\frac{Qx}{\sqrt{2}} = qx$, then,

$$K = w\sin\frac{Qx}{\sqrt{2}}(e^{qx} - e^{-qx}) \tag{137}$$

and

$$J = w\cos\frac{Qx}{\sqrt{2}}(e^{qx} + e^{-qx}) \tag{138}$$

where ψ is the phase shift expected and Ampl is the amplitude of the response that may be measured at $x = L$.

8.6 Response Analysis

Using values for the parameters involved, similar to the previous case, we plot a response curve to highlight the controlling factors. In Fig. 18, plotting response vs. $(k/\mu w)$, we see that an increase in permeability will decrease phase shift change and increase the amplitude ratio, while an increase in viscosity or frequency would increase the phase shift and decrease the amplitude.

In this model, a change in porosity also results in a change in moduli of the rock, derived from the recent developments in rock physics. Fig. 19 shows the changes due to a variation in porosity. As reported by others earlier we can now show why amplitude responses can be expected to be larger for smaller porosities.

9 A FINITE-DIFFERENCE MODEL FOR FREE SURFACE GRAVITY DRAINAGE WELL TEST ANALYSIS

This project is under the direction of Professors H. J. Ramey, Jr. and A. Correa and is conducted by Dr. F. Couri and Research Associate, J. Aasen.

The unconfined gravity flow of liquid with a free surface into a well is a classical well test problem which has not been well understood. Many authors treat this incompressible flow as compressible flow to justify the delayed yield behavior of a time-drawdown test. A finite-difference model was developed to simulate the free surface gravity flow of an unconfined single phase infinitely large reservoir into a well with storage and skin effect. The model was verified with published experimental results in sandbox models and with classical methods applied to observation wells in the groundwater literature. The simulator response was also compared with analytical approaches for wellbore pressure at late producing time.

The seepage face at the sandface and delayed yield behavior were reproduced by the model considering a small liquid compressibility and incompressible porous medium. The potential buildup (recovery) simulated by the model was quite different from drawdown behavior, contrary to conclusions found in the groundwater literature. Graphs of buildup potential vs. time,

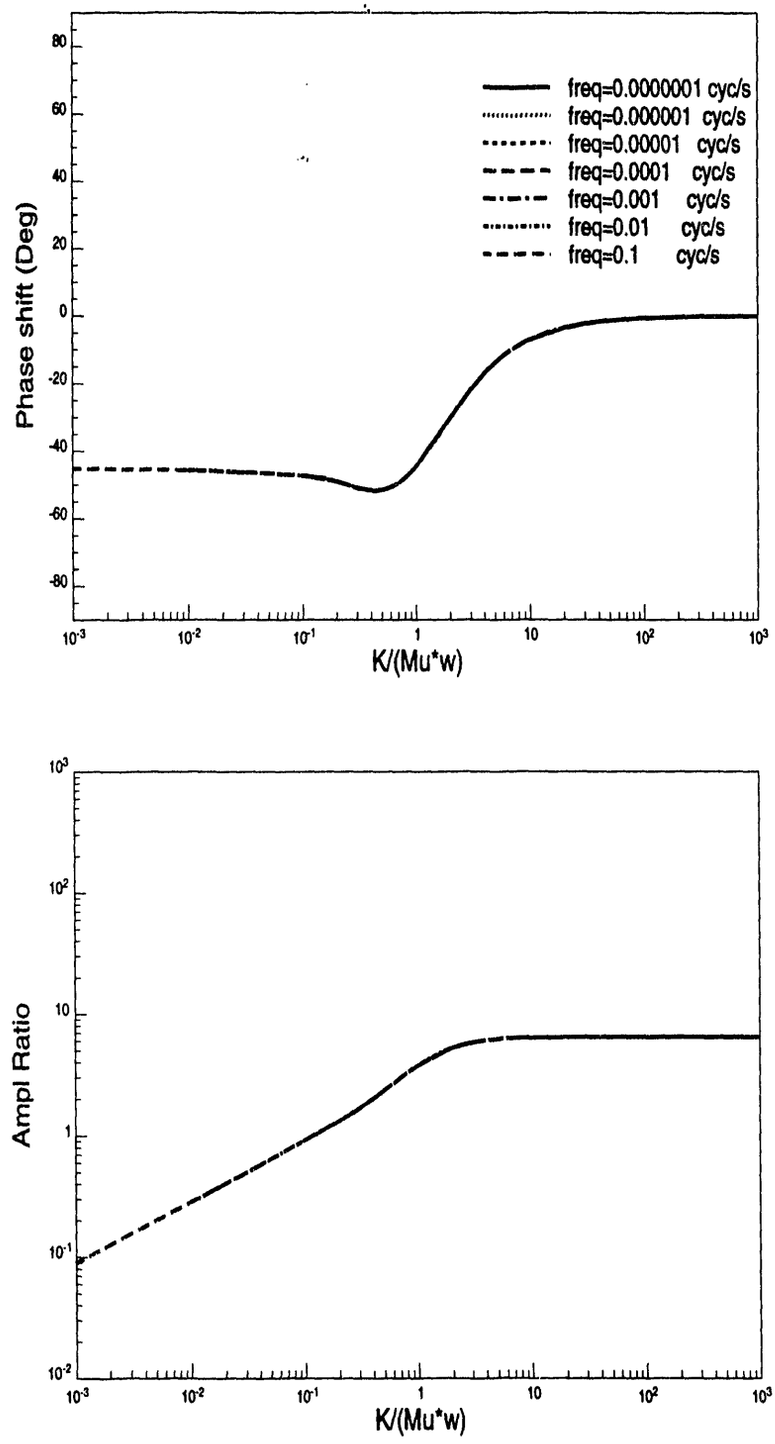

Figure 18: CaseII: Response vs. $k/\mu w$

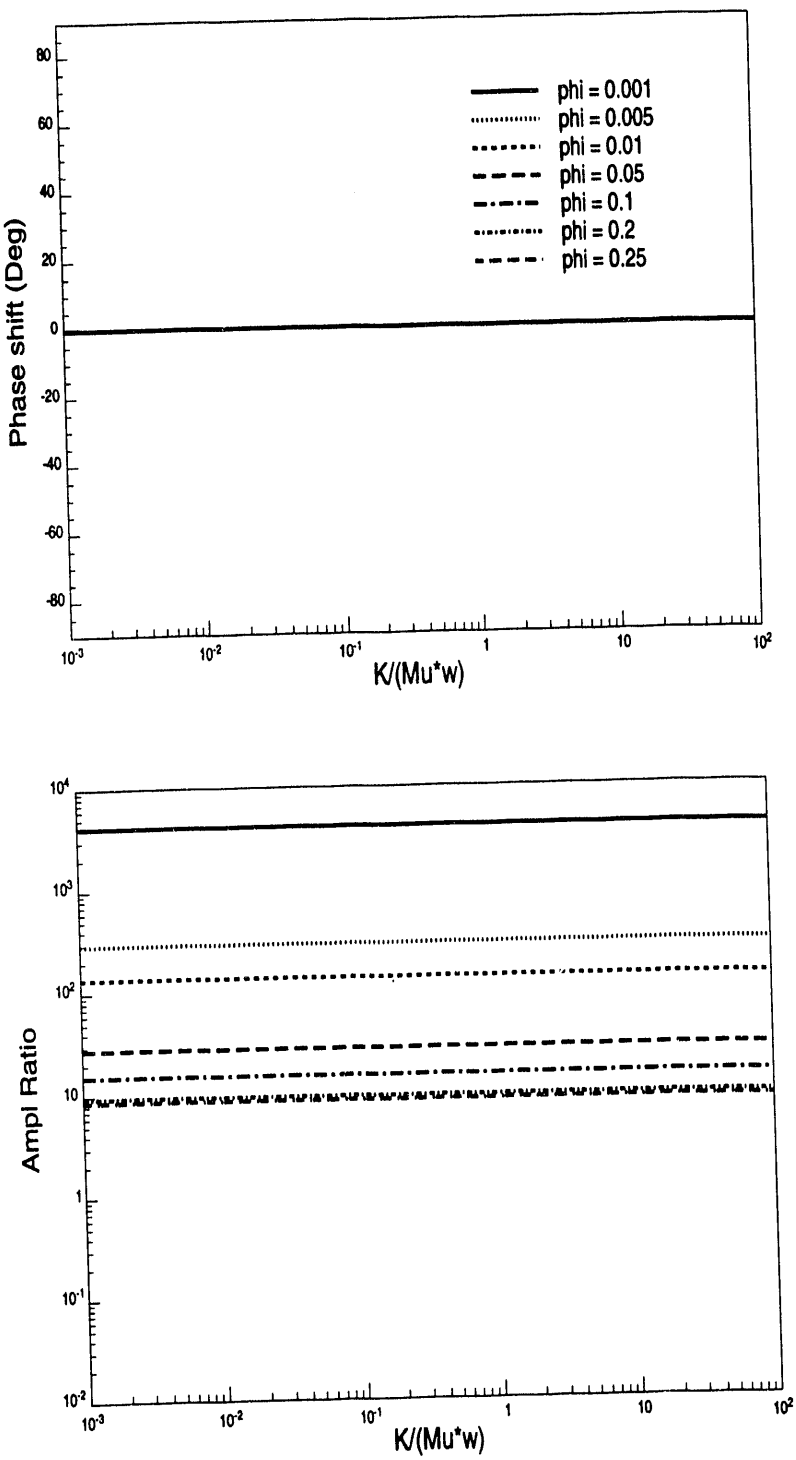

Figure 19: CaseII: Response vs. change in porosity

buildup seepage face length vs. time, and free surface head and sand bottom head radial profiles showed that the liquid refills the desaturating cone as a flat moving surface. The late time pseudo-radial behavior was only approached after exaggerated long times for pressure buildup. A dissertation on this study was presented by Dr. Francisco Couri in March 1993 and is available as Project Report No. 143.

References

- Adamson, A.W.: "Physical Chemistry of Surfaces", John Wiley and Sons, Inc., 5th ed., 1990.
- Arditty, P.C., Ramey, Jr., H.J. and Nur, A.M.: "Response of a Closed Well-Reservoir System to Stress Induced by Earth-Tides", SPE 7484, 53rd Annual Technical Conference, Houston (Oct. 1-3, 1978).
- Batchelor, G.K.: "Transport Properties of Two-Phase Materials with Random Structure", Annual Review of Fluid Mechanics, Vol. 6, (1974) 227-255.
- Bredehoeft, J.D., Cooper, H.H., and Papadopulos, I.S.: "Inertial and Storage Effects in Well-Acquifer Systems and Analog Investigations", Water Resources Research, Vol 2(4), (1966), 697-707.
- Bredehoeft, J.D.: "Response of Well-Acquifer Systems to Earth-Tides", J.Geoph Res, Vol 72(12), (June 1967), 3075-3087.
- Calhoun, J.C. and Lewis, Jr., M.: "Experiments on the Capillary Properties of Porous Solids", Trans. AIME, (1949).
- Cooper, Jr., H.H., Bredehoeft, J.D., Papadopulos, I.S, and Bennett, R.R.: "The Response of the Well-Acquifer Systems to Seismic Waves", J.Geoph.Res, Vol 70(16), (1965), 3915-3926.
- Couri, F.R.: "A Finite Difference Model for Free Surface Gravity Drainage", Ph.D. Dissertation, Stanford University, March 1993. See also SGP Report No. 143.

- Crank, J.: "The Mathematics of Diffusion", Oxford, Clarendon Press, 1964.

- Doughty, C. and Pruess, K.: "A Similarity Solution for Two-Phase Water, Air, and Heat Flow Near a Linear Heat Source in a Porous Media", Journal of Geophysical Research, Vol. 97, no. B2 (1992) 1821-1838.

- Dullien, F.A.L.: "Porous Media – Fluid Transport and Pore Structure", Academic Press, (1992) 1-574.

- Fitzgerald, S.D. and Woods, A.W.: "The Injection of Water into and Extraction of Vapour from a Geothermal Reservoir", Cambridge University, England, Unpublished report, July, 1992.

- Fitzgerald, S.D. and Woods, A.W.: "Vapour Generation in Hot Permeable Rock through Injection of Water", Proceedings: Seventeenth Workshop on Geothermal Reservoir Engineering, Stanford University, Jan., 1992.

- Gringarten, A.C. Ramey Jr., H.J.: "The Use of Source and Green's Functions in Solving Unsteady-Flow Problems in Reservoirs," SPEJ (October 1973), 285-296.

- Harr, M.S.: "Laboratory Measurement of Sorption in Porous Media", M.S. Report, Stanford Geothermal Program Report SGP-TR-138, Stanford, CA (1991).

- Hemala, M.L., and Balnaves, C.: "Tidal Effects in Petroleum Well Testing", SPE 14607, presented at SEAC, Singapore, (Jan. 28-31, 1986).

- Herkelrath, W.N., Moench, A.N., and O'Neal II, C.F.: "Laboratory Investigations of Steam Flow in a Porous Medium", Water Resources Research, Vol. 19, no. 4, (1983) 931-937.

- Hsieh, C.H. and Ramey, Jr., H.J.: "Vapor-Pressure Lowering in Geothermal Systems", SPE 9926, SPE Annual Technical Conference, Bakersfield, CA, Nov. 15, 1981.

- Leaver, J.D., Grader, A. and Ramey, Jr., H.J.: "Multiple-Well Interference Testing in the Ohaaki Geothermal Field", SPE Formation Evaluation (June 1988), 429-437.
- Melchior, P.: "The Earth Tides", 458 pp., Pergamon, New York, 1966.
- Moench, A. F.: "Simulation of Steam Transport in Vapor-Dominated Geothermal Reservoirs", USGS, no. 76-607, Menlo Park, CA, 1976.
- Moench, A. F. and Atkinson, P. F.: "Transient-Pressure Analysis in Geothermal Steam Reservoirs with an Immobile Vaporizing Liquid Phase, Geothermics", Vol. 10, no. 7, (1978) 253-264.
- Nghiem, C.P. and Ramey, Jr., H.J.: "One Dimensional Steam Flow in Porous Media", SGP Report SGP-TR-132, Stanford Geothermal Program, Stanford, CA (1991).
- Pruess, K.: "Heat Transfer in Fractured Geothermal Reservoirs with Boiling", Water Resources Research, Vol. 19, no. 1, (1983) 201-208.
- Pruess, K., Calore, C., Celati, R., and Wu, Y.S.: "An Analytical Solution for Heat Transfer at a Boiling Front Moving through a Porous Medium", Int Journal of Heat Mass Transfer, Vol. 30, no. 12, (1987) 2595-2602.
- Pruess K. and O'Sullivan M.: "Effects of Capillarity and Vapor Adsorption in the Depletion of Vapor-Dominated Geothermal Reservoirs", Proceedings: Seventeenth Workshop on Geothermal Reservoir Engineering, Stanford University, Jan. 1992.
- Stanford Geothermal Program Second Annual Technical Report, 1992.
- Stanford Geothermal Program July–Sept. Quarterly Report, 1992.
- Stanford Geothermal Program Oct.–Dec. Quarterly, Report, 1992.
- Strobel, C.J., Gulati, M.S and Ramey, Jr., H.J.: "Reservoir Limit Tests in a Naturally Fractured Reservoir - a Field Case Study Using Type Curves", JPT, Sept 1976, 1097-1106.

- Udell, K.S.: "The Thermodynamics of Evaporation and Condensation in Porous Media", SPE 10779, California Regional Meeting of SPE, San Francisco, CA, March 24-26, 1982

- Whiting, R.L. and Ramey, Jr. H.J.: "Application of Material and Energy Balances to Geothermal Steam Production", SPE 1949, SPE Annual Conference and Exhibition, Houston, TX, Oct. 1-4, 1967.

- Woods, A.W. and Fitzgerald, S.D.: "The Generation of Vapour in a Hot Rock through Injection of Cold Water", Cambridge University, England, Unpublished report, April, 1992.

DATE
FILMED
8/31/93
END